

Resummed next-to-soft corrections to rapidity distribution of Higgs boson to NNLO + NNLL

V. Ravindran, Aparna Sankar, and Surabhi Tiwari 

The Institute of Mathematical Sciences, HBNI, Taramani, Chennai 600113, India



(Received 18 June 2022; accepted 21 June 2023; published 14 July 2023)

We present the resummed predictions consisting of both soft-virtual (SV) as well as next-to-SV (NSV) threshold logarithms to all orders in perturbative QCD for the rapidity distribution of Higgs boson up to next-to-next-to-leading order plus next-to-next-to-leading-logarithmic (NNLO + NNLL) accuracy at LHC. Using our recent formalism, the resummation is carried out in the double Mellin space by restricting the NSV contributions only from diagonal gg channel. We perform the inverse Mellin transformation using the minimal prescription procedure and match it with the corresponding fixed-order results. We do a detailed analysis of the numerical impact of the resummed result. The K-factor values at different logarithmic accuracy suggest that the prediction for the rapidity distribution converges and becomes more reliable at NNLO + NNLL order. Further, we observe that the inclusion of resummed NSV contribution improves the renormalization scale uncertainty at every order in perturbation theory. However, the uncertainty due to factorization scale increases by the addition of resummed SV + NSV predictions to the fixed-order rapidity distribution.

DOI: [10.1103/PhysRevD.108.014012](https://doi.org/10.1103/PhysRevD.108.014012)

I. INTRODUCTION

There have been plethora of data available on accurate measurements of observables from LHC at CERN in recent times. This, combined with the precise theoretical predictions from various state-of-the-art computations, has facilitated establishing the Standard Model (SM) as being extremely successful in describing the physics of elementary particles. It has also helped in probing physics beyond the SM (BSM) scenarios in a very clear environment. In the next few years, the high-luminosity LHC will come into effect, which will not only increase the chances to see rare processes, but will also improve the precision of measurements. One of the most important processes at LHC is the Higgs boson production, which helps in probing the electroweak symmetry breaking and the coupling of the Higgs boson with other SM particles. The dominant channel in Higgs production is the gluon fusion process due to the large flux of gluons present in the protons at these energies. The other alternate channel is through the bottom quark annihilation, which has gained the attention of theoretical physicists in recent times due to the freedom it provides in treating the initial state bottom quarks.

The Drell-Yan (DY) production of a pair of leptons through the decay of virtual photons, Z and W bosons, at LHC is also an effective process as it helps in probing the structure of hadrons.

The measurements of inclusive and differential rates [1,2], like transverse momentum and rapidity distributions of the Higgs boson production, are very useful in understanding the symmetry breaking mechanism and Higgs boson coupling with other SM particles. Likewise, measurements [3–5] pertaining to Drell-Yan production for inclusive as well as differential rates provide pivotal information related to BSM scenarios, namely, R-parity violating supersymmetric models [6], models with Z' or with contact interactions, and large extra-dimension models [7,8]. The rapidity distributions of Drell-Yan production have also been used for a long time to calibrate the detectors and to obtain the parton distribution functions (PDFs) [9–13]. The next-to-next-to-leading order (NNLO) QCD predictions for inclusive and rapidity distribution for both Drell-Yan and Higgs boson production in gluon-gluon fusion have been known for a long time. In recent years, the next-to-next-to-next-to-leading order (N^3 LO) result for the Drell-Yan [14,15] as well as Higgs production through gluon fusion [16–18] and through bottom quark annihilation [19,20] have become available for both of these observables.

The fixed-order QCD predictions for both inclusive and differential cross sections have limitations in applicability due to the presence of various logarithms that become large

Published by the American Physical Society under the terms of the Creative Commons Attribution 4.0 International license. Further distribution of this work must maintain attribution to the author(s) and the published article's title, journal citation, and DOI. Funded by SCOAP³.

in a certain kinematic region, called the threshold region. These dominant contributions in the form of logarithms that result from the emission of soft gluons spoil the reliability of the perturbative results due to the truncation of the series. A viable solution to this problem is to systematically resum these large logarithms to all orders in perturbation theory and then supplement it with the fixed-order results, which can cover the entire kinematic region of the phase space. There are several approaches in the literature to achieve this for both inclusive and differential cross sections [21–27]. Sterman [21] and Catani and Trentadue [22] did extensive studies to achieve the resummation of these threshold large logarithms, also called soft-virtual (SV) logarithms, through the reorganization of the perturbative series. They performed the threshold resummation in the Mellin space for the inclusive case, whereas for the rapidity distribution, the formalism was extended using double Mellin moments. Using factorization properties and renormalization group (RG) invariance, one of the authors of this paper developed an all-order z space formalism to capture the threshold-enhanced contribution in the context of inclusive [27,28] as well as differential cross sections [29] of any colorless particle. This formalism was further used for Z and W^\pm case [30] using two scaling variables. It was also applied to Drell-Yan and Higgs boson production at N³LO level [20,31] and at next-to-next-to-leading order plus next-to-next-to-leading logarithmic (NNLO + NNLL) accuracy [32,33]. The threshold resummation technique has also been achieved using the soft-collinear effective theory (SCET) in momentum space for inclusive [34] as well as transverse momentum distribution [35]. The resummation for rapidity distribution using SCET formalism has been carried out in Refs. [36–38].

The threshold resummation technique that we have followed in this paper is based on Refs. [22,29,30]. Here, the resummation for the rapidity distribution is done in the two-dimensional Mellin space as the convolutions become normal products in the N space. The double Mellin variables N_1 and N_2 correspond to z_1 and z_2 in z space; hence the resummation of large logarithms becomes proportional to $\log(N_i)$ in the limit $N_i \rightarrow \infty$ ($z_i \rightarrow 1$ in z space) with $i = 1, 2$. In the large N limit, the $\log(N_i)$ combined with the strong coupling constant α_s gives order 1 terms and, therefore, truncating the series at a particular order of α_s is not possible. This difficulty is overcome by using the factorization properties, universality of the infrared (IR) contributions and the RG invariance to systematically resum these order 1 terms to all orders in perturbation theory. In this paper, we not only deal with the SV logarithms, but have included the resummed subleading threshold logarithms known as next-to-soft-virtual (NSV) logarithms as well. The importance of these collinear NSV logarithms was understood long ago and several attempts have been made so far to understand the structure of these corrections for certain inclusive [14,16,19,39] and

differential [40] observables. Unlike the SV distributions, these NSV logarithms are also present in the off-diagonal channels. The understanding of their all-order structure is still an open problem [41–53]. Recently, we have developed a formalism to systematically resum the NSV logarithms coming from diagonal channels for inclusive cross sections of various processes at LHC [54–57]. It was later extended for the case of rapidity distribution of a pair of leptons in Drell-Yan and a Higgs boson in gluon fusion as well as in bottom quark annihilation [58]. We have achieved the resummation of these NSV logarithms to all orders in perturbation theory in z as well as in the Mellin N space.

In this paper, we discuss the phenomenological importance of the resummed NSV logarithms for the production of Higgs boson via gluon fusion at LHC. We first review the theoretical framework of the formalism developed to study these logarithms along with the relevant theoretical predictions. This is followed by the comprehensive study on the numerical impact of resumming the NSV contributions at various orders in perturbation theory. Finally, we conclude the paper by providing a short discussion on our main findings.

II. THEORETICAL FRAMEWORK

We begin by considering a generic hadronic collision between two hadrons $H_{1,(2)}$ having momentum $P_{1,(2)}$ that produce a colorless final state denoted as $F(q)$ with q being its momentum,

$$H_1(P_1) + H_2(P_2) \rightarrow F(q) + X. \quad (1)$$

Here, the quantity X represents an inclusive hadronic state. The rapidity of this final colorless state F is defined through

$$y \equiv \frac{1}{2} \ln \left(\frac{P_2 \cdot q}{P_1 \cdot q} \right). \quad (2)$$

In a QCD improved parton model, the differential distribution with respect to rapidity for the colorless state F at a hadronic level for Higgs boson production through gluon fusion can be expressed as

$$\begin{aligned} \frac{d\sigma^g}{dy} &= \tilde{\sigma}_B^g(\tau, q^2) \sum_{a,b=q,\bar{q},g} \int_{x_1^0}^1 \frac{dz_1}{z_1} \int_{x_2^0}^1 \frac{dz_2}{z_2} f_a \left(\frac{x_1^0}{z_1}, \mu_F^2 \right) \\ &\times f_b \left(\frac{x_2^0}{z_2}, \mu_F^2 \right) \Delta_{d,ab}^g(z_1, z_2, q^2, \mu_F^2, \mu_R^2), \end{aligned} \quad (3)$$

where $\tilde{\sigma}_B$ is the product of the Born cross section computed in full theory with finite quark masses and the square of the Wilson coefficient C_H in the Higgs effective field theory [59,60]. Here, we have included the Wilson coefficient C_H computed in Ref. [59] as given below,

$$\begin{aligned}
C_H(a_s) = & -\frac{4a_s}{3} \left[1 + a_s(11) + a_s^2 \left(\left\{ \frac{2777}{18} + 19 \log \left(\frac{\mu_R^2}{m_t^2} \right) \right\} + n_f \left\{ -\frac{67}{6} + \frac{16}{3} \log \left(\frac{\mu_R^2}{m_t^2} \right) \right\} \right) \right. \\
& + a_s^3 \left(-\frac{2892659}{648} + \frac{3466}{9} \log \left(\frac{\mu_R^2}{m_t^2} \right) + 209 \log^2 \left(\frac{\mu_R^2}{m_t^2} \right) + \frac{897943}{144} \zeta_3 \right. \\
& + n_f \left\{ \frac{40291}{324} + \frac{1760}{27} \log \left(\frac{\mu_R^2}{m_t^2} \right) + 46 \log^2 \left(\frac{\mu_R^2}{m_t^2} \right) - \frac{110779}{216} \zeta_3 \right\} \\
& \left. \left. + n_f^2 \left\{ -\frac{6865}{486} + \frac{77}{27} \log \left(\frac{\mu_R^2}{m_t^2} \right) - \frac{32}{9} \log^2 \left(\frac{\mu_R^2}{m_t^2} \right) \right\} \right) \right], \quad (4)
\end{aligned}$$

where $a_s = \frac{\alpha_s}{4\pi}$, n_f is the number of light quark flavors and ζ_3 is the Riemann zeta function. In (3), $\bar{\sigma}_B$ explicitly depends on the masses of both the Higgs boson (m_H) and the top quark (m_t) and is renormalized at the renormalization scale μ_R . The dimensionless variable z is defined as $z = \frac{q^2}{\hat{s}}$, where \hat{s} is the square of the partonic center of mass energy and τ is defined as $\tau = q^2/S$, where S is the square of the hadronic center of mass energy. The nonperturbative functions $f_c(x_l, \mu_F^2)$ are the parton distribution functions of the colliding partons a, b with momentum fractions x_l ($l = 1, 2$). These PDFs are renormalized at the factorization scale μ_F . The other scale appearing in the above equation is the renormalization scale μ_R used for the evolution of the strong coupling constant α_s . Here, we limit our computation to the region of threshold limit or soft limit, i.e., $z \rightarrow 1$, and the corresponding contribution to the differential rapidity distribution is referred to as SV + NSV contributions. In order to define the threshold limit at the partonic level for the rapidity distribution, we choose to work with a set of symmetric scaling variables $x_{1(2)}^0$ instead of y and τ , which are related through

$$y \equiv \frac{1}{2} \ln \left(\frac{x_1^0}{x_2^0} \right) \quad \text{and} \quad \tau \equiv x_1^0 x_2^0. \quad (5)$$

In (3), $\Delta_{d,ab}^g$ are calculated perturbatively in powers of strong coupling constant a_s and are referred to as coefficient functions (CFs). Beyond leading order, the CFs contain ultraviolet and infrared divergences at the intermediate stages. The UV divergences are often removed in the $\overline{\text{MS}}$ renormalization scheme at a renormalization scale μ_R . The UV finite partonic cross sections are then left with two categories of IR divergences, namely, soft and collinear divergences. The soft divergences associated with the soft gluons get canceled between the virtual and real emission diagrams in infrared safe observables. The collinear singularities related to the collinear partons are removed by summing over degenerate final states and by mass factorization at a factorization scale μ_F . The fixed-order perturbative

results are therefore often sensitive to scales μ_R and μ_F . The CFs contain various logarithmic structures and are represented as

$$\begin{aligned}
\Delta_{d,ab}^g(z_1, z_2, q^2, \mu_F^2, \mu_R^2) \\
= \sum_{i=0}^{\infty} a_s^i(\mu_R^2) \Delta_{d,ab}^{(i),g}(z_1, z_2, q^2, \mu_F^2, \mu_R^2), \quad (6)
\end{aligned}$$

where

$$\begin{aligned}
\Delta_{d,ab}^{(i),g}(z_1, z_2, q^2, \mu_F^2, \mu_R^2) \\
= \Delta_{d,ab,\delta\delta}^{(i),g} \delta(1-z_1) \delta(1-z_2) \\
+ \sum \Delta_{d,ab,\delta\mathcal{D}_j}^{(i),g} \delta(1-z_2) \mathcal{D}_j + \sum \Delta_{d,ab,\delta\bar{\mathcal{D}}_j}^{(i),g} \delta(1-z_1) \bar{\mathcal{D}}_j \\
+ \sum \Delta_{d,ab,\mathcal{D}_j\bar{\mathcal{D}}_k}^{(i),g} \mathcal{D}_j \bar{\mathcal{D}}_k + \Delta_{d,ab,R}^{(i),g}(z_1, z_2), \quad (7)
\end{aligned}$$

$$\text{with } \mathcal{D}_i = \left[\frac{\ln^i(1-z_1)}{(1-z_1)} \right]_+, \quad \bar{\mathcal{D}}_i = \left[\frac{\ln^i(1-z_2)}{(1-z_2)} \right]_+. \quad (8)$$

The distributions \mathcal{D}_i and $\bar{\mathcal{D}}_i$ along with $\delta(1-z_1)$ and $\delta(1-z_2)$ are called the SV contributions to the infrared safe observable. These terms come from only diagonal channels. The leading contributions of the regular part $\Delta_{d,ab,R}^{(i),g}(z_1, z_2)$ near the threshold region $z_l = 1$ consist of terms of the form $\mathcal{D}_i(z_l) \ln^k(1-z_j)$ and $\delta(1-z_l) \ln^k(1-z_j)$ with $(l, j = 1, 2)$, $(i, k = 0, 1, \dots)$. These are called the NSV contributions, which come from diagonal as well as nondiagonal channels. The SV terms have been studied in great detail by one of the authors of this paper in Ref. [29]. In the next section, we explore the NSV contributions to the partonic CFs.

A. Next to SV in z space

The subleading NSV contributions present in the regular part of the partonic CFs play an important role in the precise prediction of the differential distributions. They also help in understanding the structure of beyond SV terms in the threshold expansion at higher orders. The regular part

of the CFs containing beyond SV terms is expanded around $z = 1$ in the following way:

$$\Delta_{d,ab,R}^{(i),g}(z_1, z_2) = \prod_{j=1,2} \sum_{k=0}^{2i-1} \sum_{l=0}^{\infty} \Delta_{d,ab,l,k}^{\text{reg.}(i),g} (1-z_j)^l \ln^k(1-z_j). \quad (9)$$

The NSV logarithms also demonstrate perturbative behavior like SV logarithms and therefore can be expressed in the powers of strong coupling constant a_s ,

$$\Delta_{d,ab}^{g,\text{NSV}}(z_1, z_2) = \sum_{i=0}^{\infty} a_s^i(\mu_R^2) \Delta_{d,ab}^{g,\text{NSV},(i)}(z_1, z_2). \quad (10)$$

In the threshold region near $z = 1$, $\Delta_{d,ab}^{g,\text{NSV},(i)}(z_1, z_2)$ is defined by setting $l = 0$ in (9) as

$$\Delta_{d,ab}^{g,\text{NSV},(i)}(z_1, z_2) = \prod_{j=1,2} \sum_{k=0}^{2i-1} \Delta_{d,ab,0,k}^{\text{reg.}(i),g} \ln^k(1-z_j). \quad (11)$$

$$\begin{aligned} \Psi_d^g(\mu_R^2, \mu_F^2, \bar{z}_1, \bar{z}_2, \epsilon) &= (\ln(Z_{\text{UV},g}(\hat{a}_s, \mu^2, \mu_R^2, \epsilon)))^2 + \ln |\hat{F}_g(\hat{a}_s, \mu^2, -m_H^2, \epsilon)|^2 \delta(\bar{z}_1) \delta(\bar{z}_2) + 2\Phi_d^g(\hat{a}_s, \mu^2, m_H^2, \bar{z}_1, \bar{z}_2, \epsilon) \\ &\quad - \mathcal{C} \ln \Gamma_{gg}(\hat{a}_s, \mu^2, \mu_F^2, \bar{z}_1, \epsilon) \delta(\bar{z}_2) - \mathcal{C} \ln \Gamma_{gg}(\hat{a}_s, \mu^2, \mu_F^2, \bar{z}_2, \epsilon) \delta(\bar{z}_1). \end{aligned} \quad (13)$$

The function Ψ_d^g is computed in $4 + \epsilon$ space-time dimensions in perturbative QCD and the scaling variables are shifted to $\bar{z}_1 = 1 - z_1$ and $\bar{z}_2 = 1 - z_2$. The symbol \mathcal{C} refers to the convolution and its action on any exponential of a function can be found in Ref. [54]. In Ref. [29], it has been demonstrated that Ψ_d^g can be decomposed in terms of form factor F^g , soft-collinear distribution Φ_d^g , and the diagonal Altarelli-Parisi kernels Γ_{gg} . The function $Z_{\text{UV},g}$ is the overall renormalization constant. The different terms in Ψ_d^g are UV and IR divergent. However, when these terms are combined, the divergences cancel among each other making Ψ_d^g finite and regular in the variable ϵ .

These NSV contributions are sometimes also called next-to-leading power contributions. We have recently developed a formalism in Ref. [58] to study the all-order behavior of NSV terms in rapidity distributions of any colorless particle produced in hadron colliders. Our formalism systematically includes the NSV contributions coming from only the diagonal channel. We have determined the complete NSV contributions to third order in strong coupling constant for the rapidity distributions of the Drell-Yan process and also for Higgs boson production via gluon fusion, as well as bottom quark annihilation in Ref. [58]. The all-order z space result is presented in a compact form through an integral representation. This z space integral representation is then used to resum order 1 terms in the two-dimensional Mellin space to get a reliable theoretical prediction.

The formalism uses RG invariance and the factorization properties to show that the diagonal CFs containing both SV and NSV contributions exponentiate as

$$\Delta_{d,g}^{\text{SV}+\text{NSV}} = \mathcal{C} \exp(\Psi_d^g(\mu_R^2, \mu_F^2, \bar{z}_1, \bar{z}_2, \epsilon)) \Big|_{\epsilon=0}, \quad (12)$$

where the function Ψ_d^g is given by

The soft-collinear distribution Φ_d^g containing only the SV contribution associated with the real emission has been discussed in great detail in Ref. [29]. In Ref. [58], we have presented the soft-collinear distribution Φ_d^g taking into account both SV and NSV contributions. The divergent part of the NSV contribution to Φ_d^g cancels against the collinear singularities from Altarelli-Parisi (AP) kernels Γ_{gg} [61]. Using the NSV incorporated soft-collinear distribution Φ_d^g , we get the integral representation of the finite function Ψ_d^g , which contains the all-order information of the mass-factorized differential distribution,

$$\begin{aligned} \Psi_d^g &= \frac{\delta(\bar{z}_1)}{2} \left(\int_{\mu_F^2}^{q^2 \bar{z}_2} \frac{d\lambda^2}{\lambda^2} \mathcal{P}^g(a_s(\lambda^2), \bar{z}_2) + \mathcal{Q}_d^g(a_s(q_2^2), \bar{z}_2) \right)_+ + \frac{1}{4} \left(\frac{1}{\bar{z}_1} \left\{ \mathcal{P}^g(a_s(q_{12}^2), \bar{z}_2) + 2L^g(a_s(q_{12}^2), \bar{z}_2) \right. \right. \\ &\quad \left. \left. + q^2 \frac{d}{dq^2} \left(\mathcal{Q}_d^g(a_s(q_{12}^2), \bar{z}_2) + 2\mathcal{Q}_{d,g}^f(a_s(q_{12}^2), \bar{z}_2) \right) \right\} \right)_+ + \frac{1}{2} \delta(\bar{z}_1) \delta(\bar{z}_2) \ln \left(g_{d,0}^g(a_s(\mu_F^2)) \right) + \bar{z}_1 \leftrightarrow \bar{z}_2, \end{aligned} \quad (14)$$

where $\mathcal{P}^g(a_s, \bar{z}_l) = P^g(a_s, \bar{z}_l) - 2B^g(a_s) \delta(\bar{z}_l)$, $q_l^2 = q^2(1 - z_l)$, and $q_{12}^2 = q^2 \bar{z}_1 \bar{z}_2$. The subscript $+$ indicates standard plus distribution. We consider only the diagonal parts of the AP

splitting function $P^g(a_s, \bar{z}_l)$, as nondiagonal splitting functions upon convolutions give only beyond NSV terms. The diagonal AP splitting function near $z = 1$ is given as

$$P_{gg}(z_j, a_s(\mu_F^2)) = 2 \left[B^g(a_s(\mu_F^2)) \delta(1 - z_j) + A^g(a_s(\mu_F^2)) \mathcal{D}_0(z_j) + L^g(a_s(\mu_F^2), z_j) \right], \quad (15)$$

where A^g and B^g are the cusp and collinear anomalous dimensions, respectively, and

$$L^g(a_s(\mu_F^2), z_j) \equiv C^g(a_s(\mu_F^2)) \ln(1 - z_j) + D^g(a_s(\mu_F^2)). \quad (16)$$

The cusp, the collinear anomalous dimensions, and the constants C^g and D^g are available in [57,62–64] up to third order. The constant $g_{d,0}^g$ present in Eq. (14) encapsulates the finite part of the virtual contributions and pure $\delta(\bar{z}_l)$ terms of Φ_d^g .

The function \mathcal{Q}_d^g present in Eq. (14) is expressed as

$$\mathcal{Q}_d^g(a_s, \bar{z}_l) = \frac{2}{\bar{z}_l} D_d^g(a_s) + 2\varphi_{d,g}^f(a_s, \bar{z}_l). \quad (17)$$

The functional form of the SV coefficient D_d^g is given in Eq. (7) of Ref. [32] where it is expanded in powers of strong coupling constant a_s in the limit $\epsilon \rightarrow 0$ and presented up to third order. The function $\varphi_{d,g}$ is the finite part of the NSV contribution $\varphi_{d,g}^{(i)}$ to the soft-collinear distribution given in Eq. (3) of [58] and is parametrized in terms of $\ln^k(1 - z_j)$ as

$$\begin{aligned} \varphi_{d,g}^f(a_s(\lambda^2), \bar{z}_l) &= \sum_{i=1}^{\infty} \sum_{k=0}^{\infty} \hat{a}_s^i \left(\frac{\lambda^2}{\mu^2} \right)^{\frac{i\epsilon}{2}} S_\epsilon^i \varphi_{d,g}^{(i,k)}(\epsilon) \ln^k \bar{z}_l \\ &= \sum_{i=1}^{\infty} \sum_{k=0}^i a_s^i(\lambda^2) \varphi_{d,i}^{g,(k)} \ln^k \bar{z}_l, \end{aligned} \quad (18)$$

where $S_\epsilon = \exp(\frac{\epsilon}{2}[\gamma_E - \ln(4\pi)])$ with γ_E being the Euler-Mascheroni constant. The upper limit on the sum over k is controlled by the dimensionally regularized Feynman integrals that contribute to order a_s^i . The coefficients $\varphi_{d,i}^{g,(k)}$ given in the above equation are known up to third order and listed below,

$$\begin{aligned} \varphi_{d,1}^{g,(0)} &= 2C_A, & \varphi_{d,1}^{g,(1)} &= 0, & \varphi_{d,2}^{g,(0)} &= C_A n_f \left(-\frac{136}{27} + \frac{8}{3} \zeta_2 \right) + C_A^2 \left(\frac{904}{27} - 28\zeta_3 - \frac{104}{3} \zeta_2 \right), \\ \varphi_{d,2}^{g,(1)} &= C_A n_f \left(-\frac{2}{3} \right) + C_A^2 \left(\frac{2}{3} \right), & \varphi_{d,2}^{g,(2)} &= C_A^2 (-4), \\ \varphi_{d,3}^{g,(0)} &= C_A n_f^2 \left(-\frac{232}{729} + \frac{32}{27} \zeta_3 - \frac{176}{27} \zeta_2 \right) + C_A^2 n_f \left(-\frac{80860}{729} + \frac{704}{9} \zeta_3 + \frac{11960}{81} \zeta_2 - \frac{24}{5} \zeta_2^2 \right) + C_A^3 \left(\frac{423704}{729} + 192\zeta_5 \right. \\ &\quad \left. - \frac{18188}{27} \zeta_3 - \frac{55448}{81} \zeta_2 + \frac{176}{3} \zeta_2 \zeta_3 + \frac{1384}{15} \zeta_2^2 \right) + C_F C_A n_f \left(-\frac{2158}{27} + \frac{472}{9} \zeta_3 + \frac{16}{3} \zeta_2 + \frac{32}{5} \zeta_2^2 \right), \\ \varphi_{d,3}^{g,(1)} &= C_A n_f^2 \left(\frac{56}{27} \right) + C_A^2 n_f \left(\frac{1528}{81} - 8\zeta_3 - \frac{152}{9} \zeta_2 \right) + C_A^3 \left(-\frac{18988}{81} + \frac{448}{3} \zeta_3 + \frac{752}{9} \zeta_2 \right) + C_F C_A n_f \left(4 - \frac{8}{3} \zeta_2 \right), \\ \varphi_{d,3}^{g,(2)} &= C_A n_f^2 \left(\frac{8}{27} \right) + C_A^2 n_f \left(\frac{164}{27} + \frac{2}{3} \zeta_2 \right) + C_A^3 \left(-\frac{1432}{27} + \frac{40}{3} \zeta_2 \right), \\ \varphi_{d,3}^{g,(3)} &= C_A^2 n_f \left(\frac{32}{27} \right) + C_A^3 \left(-\frac{176}{27} \right). \end{aligned} \quad (19)$$

The color factors $C_A = N_c$ and $C_F = (N_c^2 - 1)/2N_c$ for the $SU(N_c)$ gauge group. Here, n_f is the number of active flavors and ζ_i are the Riemann zeta functions. The next task is to systematically resum these SV and NSV logarithms illustrated above in the threshold region $z_l \rightarrow 1$, where they become numerically large.

B. Resummation

We have derived the analytical expression of the resummed partonic coefficient function in Ref. [58] in the double Mellin space where $z_l \rightarrow 1$ translates to large N_l

limit with $l = 1, 2$. Using the all-order integral representation of Ψ_d^g in Eq. (14) and the RG equation of a_s , the Mellin moment of Δ_d^g is expressed as

$$\Delta_{d,N_1,N_2}^g = \tilde{g}_{d,0}^g \exp(\Psi_{d,N_1,N_2}^g), \quad (20)$$

where $\Psi_{d,\bar{N}}^g$ is the double Mellin moment of the function Ψ_d^g and $\tilde{g}_{d,0}^g = \sum_{i=0}^{\infty} a_s^i \tilde{g}_{d,0,i}^g$ are the N -independent constants. Section 2.2 of [41] and Appendix A.5 of [54] contain the results required for the computation of Mellin moments of distributions as well as the regular terms in the large N_l

limit for inclusive cross section, which we have extended for the rapidity distribution case. Using these results, we computed the resummed result for $\Psi_{d,\bar{N}}^g$ and it takes the following form:

$$\begin{aligned} \Psi_{d,N_1,N_2}^g &= g_{d,1}^g(\omega) \ln N_1 \\ &+ \sum_{i=0}^{\infty} a_s^i \left(\frac{1}{2} g_{d,i+2}^g(\omega) + \frac{1}{N_1} \tilde{g}_{d,i+1}^g(\omega) \right) \\ &+ \frac{1}{N_1} \left(h_{d,0}^g(\omega, N_1) + \sum_{i=1}^{\infty} a_s^i h_{d,i}^g(\omega, \omega_1, N_1) \right) \\ &+ (N_1 \leftrightarrow N_2, \omega_1 \leftrightarrow \omega_2), \end{aligned} \quad (21)$$

where

$$\begin{aligned} h_{d,0}^g(\omega, N_l) &= h_{d,00}^g(\omega) + h_{d,01}^g(\omega) \ln N_l, \\ h_{d,i}^g(\omega, \omega_l, N_l) &= \sum_{k=0}^{i-1} h_{d,ik}^g(\omega) \ln^k N_l + \tilde{h}_{d,ii}^g(\omega, \omega_l) \ln^k N_l. \end{aligned} \quad (22)$$

Here $\omega = a_s \beta_0 \ln N_1 N_2$, $\omega_l = a_s \beta_0 \ln N_l$ for $l = 1, 2$ and $h_{d,01}^g(\omega) = 0$.

The expressions in (21) and (22) are slightly different from those in Eqs. (12) and (13) of [58], due to the explicit ω_l dependence in the diagonal terms $\tilde{h}_{d,ii}^g$, which needs an explanation. We notice that the diagonal terms $h_{d,ii}^g$ for $i \geq 2$ (or, in general, $h_{d,ic}^g$ for $c = q, g, b$, which represent the Drell-Yan process, Higgs production in gluon fusion, and bottom quark annihilation, respectively) involve only the previous order information and hence can be included in the earlier order. Taking this fact into account, we redefine the diagonal terms at each order in the following way:

$$\begin{aligned} \tilde{h}_{d,11}^g(\omega, \omega_l) &= h_{d,11}^g(\omega) + \frac{\omega_l}{\beta_0} h_{d,22}^g, \\ \tilde{h}_{d,ii}^g(\omega, \omega_l) &= \frac{\omega_l}{\beta_0} h_{d,i+1,i+1}^g, \quad \forall i \geq 2. \end{aligned} \quad (23)$$

The results of $h_{d,ii}^g$ remain the same as in [58]. We emphasize that both the definitions correctly predict the higher-order resummed terms at every logarithmic accuracy and the only difference comes in how much lower-order information is required for predicting the higher-order terms.

Working in the Mellin space has facilitated the entire exponent in Eq. (20) to be written in a compact form through the functions $g_{d,i}^g$, $\tilde{g}_{d,i}^g$, and $h_{d,i}^g$, containing both SV and NSV logarithmic contributions to all orders. Also, the use of resummed a_s allowed us to organize the series in such a way that ω is treated as order 1 at every order in perturbation theory. The integral representation in z space (14) and the resummed result in Mellin space contain exactly the same information regarding SV and NSV contributions, with the only difference being that there is no compact-looking structure in the former case. The N -independent constants $\tilde{g}_{d,0}^g$ and the SV resummation exponents $g_{d,i}^g$ have been discussed in great detail in Refs. [32,58,65,66]. Also, the explicit expressions for $\tilde{g}_{d,0}^g$ and $g_{d,i}^g$ can be found in the Supplemental Material of Ref. [58]. Here, we focus on the NSV resummation exponents, namely, $\tilde{g}_{d,i}^g$ and $h_{d,i}^g$. The coefficients $h_{d,i}^g$ depend on the NSV coefficients $\varphi_{d,c}^f$, as well as on C^g and D^g from \mathcal{P}^g . It contains a double series expansion in a_s (μ_R^2) and $\ln N_l$ and the explicit $\ln N_l$ comes from the explicit $\ln(1 - z_l)$ terms in the expansion of $\varphi_{d,g}^f$. The coefficient $h_{d,01}^g$ being proportional to C_1^g is identically zero. Hence, at order a_s^0 , there is no $(1/N_l) \ln(N_l)$ term. The results for the coefficients $\tilde{g}_{d,i}^g$ and $h_{d,i}^g$ are provided in Appendixes A and B, respectively.

The entire all-order information is embedded systematically in the resummation exponents $\tilde{g}_{d,0,i}^g$, $g_{d,i}^g(\omega)$, $\tilde{g}_{d,i}^g(\omega)$, and $h_{d,i}^g(\omega, \omega_l, N_l)$, which can be used to predict SV and NSV terms to all orders. We present Tables I and II below to demonstrate this predictive feature for the SV and NSV terms in Δ_{d,N_1,N_2}^g at a given logarithmic accuracy. In Table I, we list the predictions for the SV logarithms. The resummed exponents $\{\tilde{g}_{d,0,0}^g, g_{d,1}^g\}$ given in the first row can predict the leading SV terms $a_s^i \ln^l N_1 \ln^k N_2$ with $l + k = 2i$ ($l, k \geq 0$) for all $i > 1$, which form the tower of

TABLE I. The set of resummed exponents $\{\tilde{g}_{d,0,n}^g, g_{d,n}^g\}$ that is required to predict the tower of SV logarithms in $\Delta_{d,N_1,N_2}^{g,(n)}$ at a given logarithmic accuracy in the Mellin N space. Here, $i, j \geq 0$ and $L_l^i = \ln^i N_l$ with $l = 1, 2$.

Given Resummed exponents	Predictions: SV logarithms					Logarithmic accuracy
	$\Delta_{d,N_1,N_2}^{g,(2)}$	$\Delta_{d,N_1,N_2}^{g,(3)}$	$\Delta_{d,N_1,N_2}^{g,(4)}$	\dots	$\Delta_{d,N_1,N_2}^{g,(n)}$	
$\tilde{g}_{d,0,0}^g, g_{d,1}^g$	$\{L_1^i L_2^j\}_{i+j=4}$	$\{L_1^i L_2^j\}_{i+j=6}$	$\{L_1^i L_2^j\}_{i+j=8}$	\dots	$\{L_1^i L_2^j\}_{i+j=2n}$	LL
$\tilde{g}_{d,0,1}^g, g_{d,2}^g$	$\{L_1^i L_2^j\}_{i+j=5,4}$	$\{L_1^i L_2^j\}_{i+j=7,6}$	$\{L_1^i L_2^j\}_{i+j=9,8}$	\dots	$\{L_1^i L_2^j\}_{i+j=2n-1,2n-2}$	NLL
$\tilde{g}_{d,0,2}^g, g_{d,3}^g$	$\{L_1^i L_2^j\}_{i+j=5,4}$	$\{L_1^i L_2^j\}_{i+j=7,6}$	$\{L_1^i L_2^j\}_{i+j=9,8}$	\dots	$\{L_1^i L_2^j\}_{i+j=2n-3,2n-4}$	NNLL

TABLE II. The set of resummed exponents $\{\tilde{g}_{d,0,n}^g, g_{d,n}^g, \bar{g}_{d,n}^g, h_{d,n}^g\}$ that is required to predict the tower of NSV logarithms in $\Delta_{d,N_1,N_2}^{g,(n)}$ at a given logarithmic accuracy in the Mellin N space. Here, $i, j \geq 0$, $L_{N_1,2}^{i,j} = \frac{\ln^i N_1}{N_1} \ln^j N_2$ and $L_{N_2,1}^{i,j} = \frac{\ln^i N_2}{N_2} \ln^j N_1$.

Given	Predictions: NSV logarithms					Logarithmic accuracy
Resummed exponents	$\Delta_{d,N_1,N_2}^{g,(2)}$	$\Delta_{d,N_1,N_2}^{g,(3)}$	$\Delta_{d,N_1,N_2}^{g,(4)}$...	$\Delta_{d,N_1,N_2}^{g,(n)}$	
$\tilde{g}_{d,0,0}^g, g_{d,1}^g, \bar{g}_{d,1}^g, h_{d,0}^g$	$\left\{L_{N_1,2}^{i,j}, L_{N_2,1}^{i,j}\right\}_{i+j=3}$	$\left\{L_{N_1,2}^{i,j}, L_{N_2,1}^{i,j}\right\}_{i+j=5}$	$\left\{L_{N_1,2}^{i,j}, L_{N_2,1}^{i,j}\right\}_{i+j=7}$...	$\left\{L_{N_1,2}^{i,j}, L_{N_2,1}^{i,j}\right\}_{i+j=2n-1}$	$\overline{\text{LL}}$
$\tilde{g}_{d,0,1}^g, g_{d,2}^g, \bar{g}_{d,2}^g, h_{d,1}^g$		$\left\{L_{N_1,2}^{i,j}, L_{N_2,1}^{i,j}\right\}_{i+j=4}$	$\left\{L_{N_1,2}^{i,j}, L_{N_2,1}^{i,j}\right\}_{i+j=6}$...	$\left\{L_{N_1,2}^{i,j}, L_{N_2,1}^{i,j}\right\}_{i+j=2n-2}$	$\overline{\text{NLL}}$
$\tilde{g}_{d,0,2}^g, g_{d,3}^g, \bar{g}_{d,3}^g, h_{d,2}^g$			$\left\{L_{N_1,2}^{i,j}, L_{N_2,1}^{i,j}\right\}_{i+j=5}$...	$\left\{L_{N_1,2}^{i,j}, L_{N_2,1}^{i,j}\right\}_{i+j=2n-3}$	$\overline{\text{NNLL}}$

SV leading logarithms (LLs) and this contributes to the SV-LL resummation. When we include the functions $\{\tilde{g}_{d,0,1}^g, g_{d,2}^g\}$ given in the second row in the exponent Ψ_{d,N_1,N_2}^g along with the first set, we get two towers of next-to-leading logarithmic (NLL) SV terms $a_s^i \ln^l N_1 \ln^k N_2$ with $l+k=2i-1, 2i-2$ for all $i > 2$. By using the first and second row resummed exponents, we get the logarithms that constitute the SV-NLL resummation. In general, the resummed result with exponents $\{\tilde{g}_{d,0,n}^g, g_{d,n+1}^g\}$ along with the previous sets can predict the term $a_s^i \ln^l N_1 \ln^k N_2$ with $l+k=2n+1, 2n$ for all $i > n+1$, where $n=0, 1, 2, \dots$ and constitutes the SV- $\overline{\text{NLL}}$ resummation.

Table II gives the predictions for NSV logarithms present in Δ_{d,N_1,N_2}^g by including the resummed exponents $\{\tilde{g}_{d,i}^g, h_{d,i}^g\}$ together with the SV resummed exponents. For instance, using the first set of resummed exponents $\{\tilde{g}_{d,0,0}^g, g_{d,1}^g, \bar{g}_{d,1}^g, h_{d,0}^g\}$, we can predict the leading towers of NSV logarithms $\{a_s^i \frac{\ln^i N_1}{N_1} \ln^k N_2, a_s^i \frac{\ln^i N_2}{N_2} \ln^k N_1\}$ with $l+k=2i-1$ for all $i > 1$. These leading towers constitute the NSV- $\overline{\text{LL}}$ resummation. The second set of resummed exponents $\{\tilde{g}_{d,0,1}^g, g_{d,2}^g, \bar{g}_{d,2}^g, h_{d,1}^g\}$ in addition to the first set gives the towers of next-to-leading NSV

terms $\{a_s^i \frac{\ln^i N_1}{N_1} \ln^k N_2, a_s^i \frac{\ln^i N_2}{N_2} \ln^k N_1\}$ with $l+k=2i-2$ for all $i > 2$ and these towers contribute to the NSV- $\overline{\text{NLL}}$ resummation. In general, using the n th set $\{\tilde{g}_{d,0,n}^g, g_{d,n+1}^g, \bar{g}_{d,n+1}^g, h_{d,n}^g\}$ in addition to the previous sets, we get to predict the highest $(n+1)$ towers of NSV logarithms in N_l with $l=1, 2$, which constitute the $\overline{\text{N}^n\text{LL}}$ resummation, at every order in a_s^i for all $i > n+1$.

C. All-order prediction

In the previous section, we have shown that, using a particular set of resummed exponents at each logarithmic accuracy, we can predict certain SV and NSV logarithms in $\Delta_{d,N_1,N_2}^{g,(n)}$ at each order in the perturbation theory in the Mellin N space as depicted in Tables I and II. Here, we present the resulting predictions for the NSV logarithms up to fourth order in perturbation theory using the set of resummed exponents belonging to $\overline{\text{LL}}$, $\overline{\text{NLL}}$, and $\overline{\text{NNLL}}$ resummation as shown in Table II. Our results do not have renormalization and factorization scales explicitly, as we have set $\mu_R = \mu_F = m_H$. The SV + NSV resummed result at the leading logarithmic ($\overline{\text{LL}}$) accuracy is given by

$$\Delta_{d,N_1,N_2}^{g,\overline{\text{LL}}} = \tilde{g}_{d,0,0}^g \exp \left[\ln N_1 g_{d,1}^g(\omega) + \frac{1}{N_1} \left(\tilde{g}_{d,1}^g(\omega) + h_{d,0}^g(\omega, N_1) \right) \right] + (N_1 \leftrightarrow N_2). \quad (24)$$

The resummed exponents present in the above equation depend on one-loop anomalous dimensions and process-dependent finite coefficients obtained from fixed-order NLO results. Thus, the above equation provides leading SV and NSV logarithms at every order in perturbation theory using only one-loop information. Below, we present the predictions for the leading NSV logarithms at a_s^2 (NNLO), a_s^3 (N³LO), and a_s^4 (N⁴LO) level resulting from the $\overline{\text{LL}}$ resummation expression. In the expressions given below, $L_{N_1,2}^{i,j} = \frac{\ln^i N_1}{N_1} \ln^j N_2$, $L_{N_1}^k = \frac{\ln^k N_1}{N_1}$, and $L_l^k = \ln N_l$ with $l=1, 2$,

and γ_E is the Euler-Mascheroni constant. At a_s^2 (NNLO), we get

$$\begin{aligned} \Delta_{d,N_1,N_2}^{g,(2)} \Big|_{\text{SV+NSV-}\overline{\text{LL}}} &= \Delta_{d,N_1,N_2}^{g,(2)} \Big|_{\text{SV-}\overline{\text{LL}}} + L_{N_1}^3 \{4C_A^2\} \\ &+ L_{N_1,2}^{2,1} \{12C_A^2\} + L_{N_1,2}^{1,2} \{12C_A^2\} \\ &+ \frac{L_3^2}{N_1} \{4C_A^2\} + (N_1 \leftrightarrow N_2). \end{aligned} \quad (25)$$

By putting $N_1 = N_2 = N$ in the above prediction and taking the Mellin inverse of the resulting expression,

we obtain the result for the inclusive cross section in z space as

$$\Delta_{\text{Mellin-Inverse},z}^{g,(2)} \Big|_{\text{SV+NSV-}\overline{\text{LL}}} = \mathcal{D}_3 \{128C_A^2\} - \ln^3(1-z) \{128C_A^2\}. \quad (26)$$

The above terms are in agreement with the explicit result given in the Appendix of Ref. [67] in the threshold domain (in the limit $z \rightarrow 1$) for $\mu = m$.

At a_s^3 (N^3LO), we obtain

$$\begin{aligned} \Delta_{d,N_1,N_2}^{g,(3)} \Big|_{\text{SV+NSV-}\overline{\text{LL}}} &= \Delta_{d,N_1,N_2}^{g,(3)} \Big|_{\text{SV-}\overline{\text{LL}}} + L_{N_1}^5 \{4C_A^3\} + L_{N_1,2}^{4,1} \{20C_A^3\} \\ &+ L_{N_1,2}^{3,2} \{40C_A^3\} + L_{N_1,2}^{2,3} \{40C_A^3\} \\ &+ L_{N_1,2}^{1,4} \{20C_A^3\} + \frac{L_2^5}{N_1} \{4C_A^3\} + (N_1 \leftrightarrow N_2). \end{aligned} \quad (27)$$

Now, following the same method that we applied on the prediction at a_s^2 order, the inclusive results in z space are given by

$$\Delta_{\text{Mellin-Inverse},z}^{g,(3)} \Big|_{\text{SV+NSV-}\overline{\text{LL}}} = \mathcal{D}_5 \{512C_A^3\} - \ln^5(1-z) \{512C_A^3\}. \quad (28)$$

The above terms in z space are in agreement with the explicit computation in Ref. [68] in the threshold domain (in the limit $z \rightarrow 1$). We have also verified the agreement of the above SV and NSV terms with the results obtained in Refs. [24,50], respectively.

Expanding Eq. (24) up to a_s^4 (N^4LO), we obtain

$$\begin{aligned} \Delta_{d,N_1,N_2}^{g,(4)} \Big|_{\text{SV+NSV-}\overline{\text{LL}}} &= \Delta_{d,N_1,N_2}^{g,(4)} \Big|_{\text{SV-}\overline{\text{LL}}} + L_{N_1}^7 \left\{ \frac{8}{3} C_A^4 \right\} + L_{N_1,2}^{6,1} \left\{ \frac{56}{3} C_A^4 \right\} \\ &+ L_{N_1,2}^{5,2} \{56C_A^4\} + L_{N_1,2}^{4,3} \left\{ \frac{280}{3} C_A^4 \right\} + L_{N_1,2}^{3,4} \left\{ \frac{280}{3} C_A^4 \right\} \\ &+ L_{N_1,2}^{2,5} \{56C_A^4\} + L_{N_1}^{1,6} \left\{ \frac{56}{3} C_A^4 \right\} + \frac{L_2^7}{N_1} \left\{ \frac{8}{3} C_A^4 \right\} \\ &+ (N_1 \leftrightarrow N_2). \end{aligned} \quad (29)$$

If we put $N_1 = N_2 = N$ in the above expression and do the Mellin inverse transformation on the resulting expression, it takes the following form in z space for the inclusive cross section at fourth order:

$$\Delta_{\text{Mellin-Inverse},z}^{g,(4)} \Big|_{\text{SV+NSV-}\overline{\text{LL}}} = \mathcal{D}_7 \left\{ \frac{4096}{3} C_A^4 \right\} - \ln^7(1-z) \left\{ \frac{4096}{3} C_A^4 \right\}. \quad (30)$$

Here, the distribution part \mathcal{D}_7 is already computed in Ref. [28], whereas the NSV part $\ln^7(1-z)$ is in agreement with the prediction obtained using the physical kernel approach in Ref. [50].

We next look at the expression for the SV + NSV resummed result at next-to-leading logarithmic ($\overline{\text{NLL}}$) accuracy given below,

$$\begin{aligned} \Delta_{d,N_1,N_2}^{g,\overline{\text{NLL}}} &= (\tilde{g}_{d,0,0}^g + a_s \tilde{g}_{d,0,1}^g) \exp \left[\ln N_1 g_{d,1}^g(\omega) + g_{d,2}^g(\omega) + \frac{1}{N_1} \left(\tilde{g}_{d,1}^g(\omega) + a_s \tilde{g}_{d,2}^g(\omega) + h_{d,0}^g(\omega, N_1) \right. \right. \\ &\left. \left. + a_s h_{d,1}^g(\omega, \omega_1, N_1) \right) \right] + (N_1 \leftrightarrow N_2, \omega_1 \leftrightarrow \omega_2). \end{aligned} \quad (31)$$

At $\overline{\text{NLL}}$ accuracy, the resummed exponents depend on the anomalous dimensions expanded up to two loops and the finite process-dependent SV and NSV coefficients obtained from fixed-order results at NNLO accuracy. The above equation provides next-to-leading SV and NSV logarithms at every order in perturbation theory using the information embedded in two-loop results. The next-to-leading NSV logarithms at a_s^3 (N^3LO) are given as

$$\begin{aligned} \Delta_{d,N_1,N_2}^{g,(3)} \Big|_{\text{SV+NSV-}\overline{\text{NLL}}} &= \Delta_{d,N_1,N_2}^{g,(3)} \Big|_{\text{SV+NSV-}\overline{\text{LL}}} + \Delta_{d,N_1,N_2}^{g,(3)} \Big|_{\text{SV-}\overline{\text{NLL}}} + L_{N_1}^4 \left\{ \left(\frac{326}{9} + 40\gamma_E \right) C_A^3 - \frac{20}{9} C_A^2 n_f \right\} \\ &+ L_{N_1,2}^{3,1} \left\{ \left(\frac{1160}{9} + 160\gamma_E \right) C_A^3 - \frac{80}{9} C_A^2 n_f \right\} + L_{N_1,2}^{2,2} \left\{ \left(\frac{484}{3} + 240\gamma_E \right) C_A^3 - \frac{40}{3} C_A^2 n_f \right\} \\ &+ L_{N_1,2}^{1,3} \left\{ \left(\frac{728}{9} + 160\gamma_E \right) C_A^3 - \frac{80}{9} C_A^2 n_f \right\} + \frac{L_2^4}{N_1} \left\{ \left(\frac{110}{9} + 40\gamma_E \right) C_A^3 - \frac{20}{9} C_A^2 n_f \right\} + (N_1 \leftrightarrow N_2). \end{aligned} \quad (32)$$

Now, by putting $N_1 = N_2 = N$ in the above expression and taking the Mellin inverse, we obtain the results for the inclusive cross section in z space as

$$\begin{aligned} \Delta_{\text{Mellin-Inverse},z}^{g,(3)} \Big|_{\text{SV+NSV-NLL}} &= \Delta_{\text{Mellin-Inverse},z}^{g,(3)} \Big|_{\text{SV+NSV-LL}} + \mathcal{D}_4 \left\{ \frac{1280}{9} C_A^2 n_f - \frac{7040}{9} C_A^3 \right\} + \mathcal{D}_3 \left\{ \left(\frac{59200}{27} - 3584\zeta_2 \right) C_A^3 \right. \\ &\quad \left. + \frac{256}{27} C_A n_f^2 - \frac{10496}{27} C_A^2 n_f \right\} + \ln^4(1-z) \left\{ \frac{22592}{9} C_A^3 - \frac{1280}{9} C_A^2 n_f \right\}. \end{aligned} \quad (33)$$

We compare the above terms in z space with the explicit results computed in Ref. [68], and they are in agreement in the threshold domain (in the limit $z \rightarrow 1$). Further, the above SV and NSV terms are also in agreement with the results presented in Refs. [24,50], respectively. At a_s^4 (N^4 LO), we find

$$\begin{aligned} \Delta_{d,N_1,N_2}^{g,(4)} \Big|_{\text{SV+NSV-NLL}} &= \Delta_{d,N_1,N_2}^{g,(4)} \Big|_{\text{SV+NSV-LL}} + \Delta_{d,N_1,N_2}^{g,(4)} \Big|_{\text{SV-NLL}} + L_{N_1}^6 \left\{ \left(\frac{370}{9} + \frac{112}{3} \gamma_E \right) C_A^4 - \frac{28}{9} C_A^3 n_f \right\} \\ &\quad + L_{N_1,2}^{5,1} \left\{ \left(\frac{692}{3} + 224\gamma_E \right) C_A^4 - \frac{56}{3} C_A^3 n_f \right\} + L_{N_1,2}^{4,2} \left\{ \left(\frac{1586}{3} + 560\gamma_E \right) C_A^4 - \frac{140}{3} C_A^3 n_f \right\} \\ &\quad + L_{N_1,2}^{3,3} \left\{ \left(\frac{5672}{9} + \frac{2240}{3} \gamma_E \right) C_A^4 - \frac{560}{9} C_A^3 n_f \right\} + L_{N_1,2}^{2,4} \left\{ \left(\frac{1226}{3} + 560\gamma_E \right) C_A^4 - \frac{140}{3} C_A^3 n_f \right\} \\ &\quad + L_{N_1,2}^{1,5} \left\{ \left(\frac{404}{3} + 224\gamma_E \right) C_A^4 - \frac{56}{3} C_A^3 n_f \right\} + \frac{L_2^6}{N_1} \left\{ \frac{154}{9} C_A^4 - \frac{28}{9} C_A^3 n_f + \frac{112}{3} \gamma_E C_A^4 \right\} + (N_1 \leftrightarrow N_2). \end{aligned} \quad (34)$$

Now, the inclusive result corresponding to the above expression in z space is as follows:

$$\begin{aligned} \Delta_{\text{Mellin-Inverse},z}^{g,(4)} \Big|_{\text{SV+NSV-NLL}} &= \Delta_{\text{Mellin-Inverse},z}^{g,(4)} \Big|_{\text{SV+NSV-LL}} + \mathcal{D}_6 \left\{ \frac{7168}{9} C_A^3 n_f - \frac{39424}{9} C_A^4 \right\} \\ &\quad + \mathcal{D}_5 \left\{ \frac{4096}{27} C_A^2 n_f^2 - \frac{91136}{27} C_A^3 n_f + \left(\frac{432640}{7} - 23552\zeta_2 \right) C_A^4 \right\} \\ &\quad + \ln^6(1-z) \left\{ \frac{98560}{9} C_A^4 - \frac{7168}{9} C_A^3 n_f \right\}. \end{aligned} \quad (35)$$

Here, we have reproduced the distribution part $\{\mathcal{D}_6, \mathcal{D}_5\}$ as given in Ref. [28], while the NSV part $\ln^6(1-z)$ is in agreement with the prediction obtained using the physical kernel approach in Ref. [50].

At last, we provide the predictions resulting from the $\overline{\text{NNLL}}$ resummation. The expression used to obtain the results at this logarithmic accuracy is given as

$$\begin{aligned} \Delta_{d,N_1,N_2}^{g,\overline{\text{NNLL}}} &= (\tilde{g}_{d,0,0}^g + a_s \tilde{g}_{d,0,1}^g + a_s^2 \tilde{g}_{d,0,2}^g) \exp \left[\ln N_1 g_{d,1}^g(\omega) + g_{d,2}^g(\omega) + a_s g_{d,3}^g(\omega) \right. \\ &\quad \left. + \frac{1}{N_1} \left(\tilde{g}_{d,1}^g(\omega) + a_s \tilde{g}_{d,2}^g(\omega) + a_s^2 \tilde{g}_{d,3}^g(\omega) + h_{d,0}^g(\omega, N_1) + a_s h_{d,1}^g(\omega, \omega_1, N_1) + a_s^2 h_{d,2}^g(\omega, \omega_1, N_1) \right) \right] \\ &\quad + (N_1 \leftrightarrow N_2, \omega_1 \leftrightarrow \omega_2). \end{aligned} \quad (36)$$

We note that the $\overline{\text{NNLL}}$ resummation requires the three-loop information coming from anomalous dimensions at third order in the strong coupling constant and also from the third-order SV and NSV finite coefficients obtained from N^3 LO results. We provide the prediction for the next-to-next-to-leading NSV logarithms at a_s^4 as given below,

$$\begin{aligned}
\Delta_{d,N_1,N_2}^{g,(4)} \Big|_{\text{SV+NSV-}\overline{\text{NNLL}}} &= \Delta_{d,N_1,N_2}^{g,(4)} \Big|_{\text{SV+NSV-}\overline{\text{NLL}}} + \Delta_{d,N_1,N_2}^{g,(4)} \Big|_{\text{SV-}\overline{\text{NNLL}}} \\
&+ L_{N_1}^5 \left\{ \frac{32}{27} C_A^2 n_f^2 - \left(\frac{1172}{27} + \frac{112}{3} \gamma_E \right) C_A^3 n_f + \left(\frac{2024}{9} + \frac{1432}{3} \gamma_E + 224 \gamma_E^2 + 40 \zeta_2 \right) C_A^4 \right\} \\
&+ L_{N_1,2}^{4,1} \left\{ \frac{160}{27} C_A^2 n_f^2 - \left(\frac{5608}{27} + \frac{560}{3} \gamma_E \right) C_A^3 n_f + \left(\frac{9604}{9} + \frac{6632}{3} \gamma_E + 1120 \gamma_E^2 + 200 \zeta_2 \right) C_A^4 \right\} \\
&+ L_{N_1,2}^{3,2} \left\{ \frac{320}{27} C_A^2 n_f^2 - \left(\frac{10568}{27} + \frac{1120}{3} \gamma_E \right) C_A^3 n_f + \left(\frac{17912}{9} + \frac{12016}{3} \gamma_E + 2240 \gamma_E^2 + 400 \zeta_2 \right) C_A^4 \right\} \\
&+ L_{N_1,2}^{2,3} \left\{ \frac{320}{27} C_A^2 n_f^2 - \left(\frac{9712}{27} + \frac{1120}{3} \gamma_E \right) C_A^3 n_f + \left(\frac{48704}{27} + \frac{10576}{3} \gamma_E + 2240 \gamma_E^2 + 400 \zeta_2 \right) C_A^4 \right\} \\
&+ L_{N_1,2}^{1,4} \left\{ \frac{160}{27} C_A^2 n_f^2 - \left(\frac{4292}{27} + \frac{560}{3} \gamma_E \right) C_A^3 n_f + \left(\frac{21088}{27} + \frac{4472}{3} \gamma_E + 1120 \gamma_E^2 + 200 \zeta_2 \right) C_A^4 \right\} \\
&+ \frac{L_1^5}{N_1} \left\{ \frac{32}{27} C_A^2 n_f^2 - \left(\frac{712}{27} + \frac{112}{3} \gamma_E \right) C_A^3 n_f + \left(\frac{3380}{27} + \frac{712}{3} \gamma_E + 224 \gamma_E^2 + 40 \zeta_2 \right) C_A^4 \right\}. \quad (37)
\end{aligned}$$

Further, the inclusive result corresponding to the above expression in z space reads as

$$\begin{aligned}
\Delta_{\text{Mellin-Inverse},z}^{g,(4)} \Big|_{\text{SV+NSV-}\overline{\text{NNLL}}} &= \Delta_{\text{Mellin-Inverse},z}^{g,(4)} \Big|_{\text{SV+NSV-}\overline{\text{NLL}}} + \mathcal{D}_4 \left\{ \frac{256}{7} C_A n_f^3 - \frac{17024}{27} C_A^2 n_f^2 + \frac{1280}{3} C_A^2 C_f n_f \right. \\
&+ \left. \left(\frac{26048}{3} - \frac{94720}{9} \zeta_2 \right) C_A^3 n_f + \left(\frac{-838112}{27} + \frac{313600}{3} \zeta_3 + \frac{520960}{9} \zeta_2 \right) C_A^4 \right\} \\
&+ \mathcal{D}_3 \left\{ -\frac{2560}{81} C_A n_f^3 + \frac{640}{9} C_A C_f n_f^2 + \left(\frac{308608}{243} - \frac{12800}{9} \zeta_2 \right) C_A^2 n_f^2 \right. \\
&+ \left. \left(\frac{-50368}{9} + 4096 \zeta_3 \right) C_A^2 C_f n_f + \left(\frac{-4338368}{243} + \frac{94208}{3} \zeta_3 + \frac{248320}{9} \zeta_2 \right) C_A^3 n_f \right. \\
&+ \left. \left(\frac{13802368}{243} - \frac{585728}{3} \zeta_3 - \frac{1107584}{9} \zeta_2 - \frac{80896}{5} \zeta_2^2 \right) C_A^4 \right\} \\
&+ \ln^5(1-z) \left\{ \left(-\frac{298240}{9} + 23552 \zeta_2 \right) C_A^4 + \frac{174208}{27} C_A^3 n_f - \frac{4096}{27} C_A^2 n_f^2 \right\}. \quad (38)
\end{aligned}$$

We have reproduced the distribution part $\{\mathcal{D}_4, \mathcal{D}_3\}$ as presented in Ref. [28], and the NSV logarithm $\ln^5(1-z)$ is found to be in agreement with the prediction obtained using the physical kernel approach in Ref. [50]. We have also checked the inclusive predictions that result from the expansion of the $\overline{\text{NNLL}}$ expression given in Eq. (36) upon putting $N_1 = N_2 = N$ and taking the Mellin inversion up to a_s^3 . It has been found that the expansion of $\overline{\text{NNLL}}$ yields the complete SV [$\delta(1-z)$ and \mathcal{D}_j with $j = 0, 1, 2, 3$] and NSV [$\ln^k(1-z)$ with $k = 0, 1, 2, 3$] terms present in the inclusive results in the threshold domain up to a_s^2 as given in Ref. [28]. At a_s^3 , the $\overline{\text{NNLL}}$ expression yields all the plus distributions except \mathcal{D}_0 and the NSV logarithms $\ln^k(1-z)$ for $k = 3, 4, 5$ as computed in Ref. [68] in the threshold limit.

III. PHENOMENOLOGY

This section presents a detailed study on the numerical impact of resummed SV + NSV corrections to $\overline{\text{NNLL}}$

accuracy for the rapidity distribution of the Higgs boson production in gluon fusion at the LHC. To distinguish between the SV and SV + NSV resummed results, the NSV included resummed results have been denoted by $\overline{\text{N}^{\text{NLL}}}$ for the n th level logarithmic accuracy. We do the analysis for center of mass energy $\sqrt{S} = 13$ TeV with the Higgs mass $m_H = 125$ GeV, top quark pole mass $m_t = 173.3$ GeV, and Fermi constant $G_F = 4541.63$ pb. The numerical values for the aforementioned parameters are taken from the Particle Data Group 2020 [69]. The fixed-order rapidity distributions have been obtained using a publicly available code FEHIP [70]. An in-house FORTRAN code has been used to perform the double Mellin inversion for the resummed contributions. We have used minimal prescription [71] to deal with the Landau pole in the Mellin inversion routines. The PDFs used are taken from the LHAPDF [72] routine using the MMHT2014(68cl) [10] parton distribution set. The strong coupling constant a_s is provided using the LHAPDF interface with $n_f = 5$ active massless quark

flavors throughout. The Mellin space PDFs ($f_{i,N}$) can be obtained by using QCD-PEGASUS [73]. However, we follow the technique given in [22,74] to directly deal with PDFs in the z space. The resummed results are matched to the fixed-order result in order to avoid any double counting of threshold logarithms and is given as

$$\begin{aligned} \frac{d\sigma^{g,\overline{\text{N}}^{\text{LO}}+\overline{\text{N}}^{\text{LL}}}}{dy} &= \frac{d\sigma^{g,\overline{\text{N}}^{\text{LO}}}}{dy} + \tilde{\sigma}_{\text{B}}^g \int_{c_1-i\infty}^{c_1+i\infty} \frac{dN_1}{2\pi i} \int_{c_2-i\infty}^{c_2+i\infty} \frac{dN_2}{2\pi i} (\tau)^{-N_1-N_2} \delta_{ab} f_{a,N_1}(\mu_F^2) f_{b,N_2}(\mu_F^2) \\ &\times \left(\Delta_{d,N_1,N_2}^g \Big|_{\overline{\text{N}}^{\text{LL}}} - \Delta_{d,N_1,N_2}^g \Big|_{\overline{\text{N}}^{\text{LO}}} \right). \end{aligned} \quad (39)$$

Here, $\tilde{\sigma}_{\text{B}}^g$ is the product of the Born cross section computed in full theory with finite quark masses and the square of the Wilson coefficient in the Higgs effective field theory. The contour c_i in the Mellin inversion can be chosen according to minimal prescription [71] procedure. The first term in Eq. (39) encapsulates the fixed-order contributions up to $\overline{\text{N}}^{\text{LO}}$ accuracy and the second term corresponds to the resummed result at $\overline{\text{N}}^{\text{LL}}$ accuracy obtained by taking the difference between the resummed result and the same truncated at order a_s^n . Therefore, the second term contains the SV + NSV resummed contributions to all orders in perturbation theory starting from a_s^{n+1} onward.

We have calculated the percentage contribution of SV distributions and NSV logarithms to the Born cross section at various orders in Table 2 of Ref. [57] at the central scale $\mu_R = \mu_F = m_H$ for the inclusive cross section of Higgs boson production in gluon fusion. Similar percentages have been computed for the Drell-Yan process, as well in Ref. [56] at the central scale $\mu_R = \mu_F = 200$ GeV. Our analysis showed that, for both the cases, the phenomenological relevance of NSV contributions increase with each order in the perturbation theory. In the case of Higgs boson production, the gg channel being the dominant contributor gives us an additional motivation to study NSV logarithms, as our formalism resums these collinear logarithms coming from the diagonal channel only. Recently, we carried out the phenomenological study for the rapidity distribution of the Drell-Yan process [75] and demonstrated that the NSV contribution plays an important role for rapidity distribution as well. Similarly, we expect the same trends to follow for the rapidity distribution of Higgs boson production through gluon fusion. Now, we ask the following questions to understand the importance of NSV terms and also to shed some light on the role of beyond NSV terms in the rapidity distribution of Higgs boson production.

- (i) How is the behavior of fixed-order rapidity distribution altered with the inclusion of SV + NSV resummed terms?
- (ii) What is the change in the sensitivity of the result on unphysical scales μ_R and μ_F when NSV logarithms from the dominant gg channel are included?
- (iii) How much is the impact of SV + NSV resummed results on the rapidity distribution in comparison to the well established SV predictions?

We will explore the above questions in the subsequent sections. We have done all the analysis for the central scale $\mu_R = \mu_F = m_H/2$ at 13 TeV LHC. The resummation scheme chosen for the phenomenological discussion in this section is \overline{N} exponentiation. Note that in Appendixes A and B, we have provided the expressions for $\tilde{g}_{d,i}^g$ and $h_{d,i}^g$ in the N exponentiation scheme, which can be converted to the \overline{N} exponentiation scheme by setting all the γ_E terms to zero and replacing all the $\ln N_1 N_2$ terms by $\ln \overline{N}_1 \overline{N}_2$, as well as all the $\omega(\omega_l)$ terms by $\bar{\omega} = a_s \beta_0 \ln \overline{N}_1 \overline{N}_2$ ($\bar{\omega}_l = a_s \beta_0 \ln \overline{N}_l$). Here, $\overline{N}_l = \exp(\gamma_E) N_l$ for $l = 1, 2$ and γ_E is the Euler-Mascheroni constant. The N -independent constants $\tilde{g}_{d,0}^g$ given in Eq. (12) can be obtained in \overline{N} exponentiation from their counterparts in the standard N exponentiation approach by simply putting the γ_E terms equal to zero. This choice of central scale and resummation scheme is inspired by the analysis done in Ref. [57] for the inclusive cross section of the Higgs boson production through gluon fusion. Also, the fixed-order results contain contributions from all the channels, whereas the resummed results contain distributions and logarithms coming from the diagonal gg channel only. The NSV logarithms resulting from the off-diagonal qg channel are not included in our formalism. Let us start the next section by analyzing the effect of the SV + NSV resummed result on the fixed-order predictions for the rapidity distribution.

A. Fixed-order vs resummed results

This section presents the detailed study on the numerical relevance of SV + NSV resummed contributions at $\overline{\text{LL}}$, $\overline{\text{NLL}}$, and $\overline{\text{NNLL}}$ matched with the corresponding fixed-order results for the rapidity distribution using Eq. (39). We investigate the enhancement of the SV + NSV resummed matched result with the fixed-order counterpart. We also demonstrate the impact of resummation of NSV logarithms in the diagonal channel on the sensitivity of the fixed-order result with respect to the unphysical scales μ_R and μ_F .

We begin by studying the quantitative impact of the SV + NSV resummed rapidity distribution through the K factors defined as

$$K = \frac{\frac{d\sigma}{dy}(\mu_R = \mu_F = m_H/2)}{\frac{d\sigma^{\text{LO}}}{dy}(\mu_R = \mu_F = m_H/2)}, \quad (40)$$

TABLE III. K-factor values of fixed-order and resummed results at the central scale $\mu_R = \mu_F = m_H/2$.

y	$K_{\text{LO}+\overline{\text{LL}}}$	K_{NLO}	$K_{\text{NLO}+\overline{\text{NLL}}}$	K_{NNLO}	$K_{\text{NNLO}+\overline{\text{NNLL}}}$
0–0.4	1.775	1.782	1.854	2.092	2.030
0.4–0.8	1.776	1.755	1.828	2.079	2.019
0.8–1.2	1.796	1.725	1.804	2.031	1.973
1.2–1.6	1.812	1.679	1.763	1.959	1.904
1.6–2.0	1.853	1.616	1.711	1.897	1.849
2.0–2.4	1.891	1.535	1.640	1.794	1.752

where the renormalization (μ_R) and factorization (μ_F) scales have been set at $m_H/2 = 62.5$ GeV. We provide Table III to present K-factor values of fixed-order as well as SV + NSV resummed results for benchmark rapidity values. We find that there is an enhancement of 77.5% and 4.04% when the resummed SV + NSV logarithms at $\overline{\text{LL}}$ and $\overline{\text{NLL}}$ are added to LO and NLO, respectively, at the central rapidity region. However, the rapidity distribution decreases by 2.96% when we include $\overline{\text{NNLL}}$ to NNLO at the central rapidity region. This suggests better perturbative convergence at the NNLO + $\overline{\text{NNLL}}$ level. We further observe that the percentage enhancement in the rapidity distribution at NNLO + $\overline{\text{NNLL}}$ over NLO + $\overline{\text{NLL}}$ is less than the enhancement when we go from NLO to NNLO accuracy for a wide range of rapidity values. This indicates that the inclusion of resummed SV + NSV logarithms makes the perturbative predictions more reliable. The above analysis based on the K-factor values demonstrates

that the SV + NSV resummed results bring substantial percentage correction to the fixed-order results and also improve the perturbative convergence and reliability of the predictions. Now, we proceed to see the dependence of resummed results on the renormalization and factorization scales.

1. Seven-point scale variation of the resummed result

The truncation of the perturbative series to a certain order of accuracy plagues the fixed-order as well as resummed predictions with the dependence on unphysical scales, namely, renormalization (μ_R) and factorization (μ_F) scales. Here, we assess the change in uncertainty with respect to these unphysical scales when the SV + NSV resummed contributions are added to the fixed-order results. We use the standard canonical seven-point variation approach where $\{\mu_R, \mu_F\}$ is varied in the range $\{m_H/4, m_H\}$, keeping the ratio $\frac{\mu_R}{\mu_F}$ not larger than 2 and smaller than 1/2. Figure 1 shows the bin-integrated rapidity distribution of the Higgs boson for fixed-order as well as SV + NSV resummed predictions at various orders in perturbation theory. We plot the seven-point scale uncertainties of the fixed-order result up to NNLO in the left panel and for the SV + NSV resummed predictions up to NNLO + $\overline{\text{NNLL}}$ in the right panel around the central scale $\mu_R = \mu_F = m_H/2$ for 13 TeV LHC. We observe that there is a significant enhancement of 77.51% and 4.05% at LO and NLO accuracy by the addition of $\overline{\text{LL}}$ and $\overline{\text{NLL}}$ contributions at the central rapidity region. However, the inclusion of

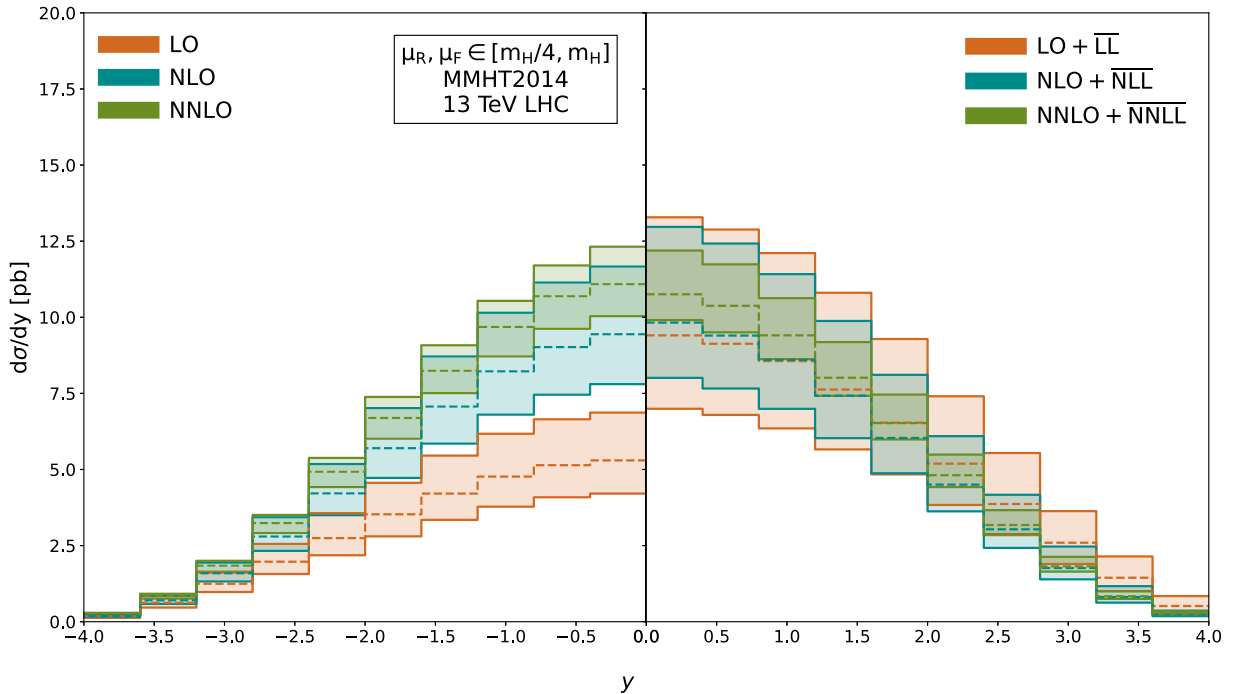


FIG. 1. Comparison of seven-point scale variation between fixed-order and SV + NSV resummed results for 13 TeV LHC. The dashed lines refer to the corresponding central scale values at each order.

TABLE IV. Values of resummed rapidity distribution at various orders in comparison to the fixed-order results in picobarn at the central scale $\mu_R = \mu_F = m_H/2$ for 13 TeV LHC.

y	LO	LO + $\overline{\text{LL}}$	NLO	NLO + $\overline{\text{NLL}}$	NNLO	NNLO + $\overline{\text{NNLL}}$
0–0.4	5.2987 ^{+1.57} _{-1.089}	9.406 ^{+3.878} _{-2.411}	9.4432 ^{+2.223} _{-1.639}	9.8252 ^{+3.144} _{-1.816}	11.0873 ^{+1.230} _{-1.051}	10.7559 ^{+1.437} _{-0.849}
0.4–0.8	5.1408 ^{+1.509} _{-1.054}	9.1303 ^{+3.752} _{-2.338}	9.0205 ^{+2.121} _{-1.563}	9.3991 ^{+3.023} _{-1.739}	10.6907 ^{+1.011} _{-1.068}	10.3777 ^{+1.361} _{-0.872}
0.8–1.2	4.7667 ^{+1.407} _{-0.988}	8.561 ^{+3.548} _{-2.211}	8.2239 ^{+1.925} _{-1.422}	8.601 ^{+2.815} _{-1.608}	9.6837 ^{+0.855} _{-0.969}	9.407 ^{+1.222} _{-0.783}
1.2–1.6	4.2089 ^{+1.248} _{-0.864}	7.626 ^{+3.179} _{-1.967}	7.0677 ^{+1.645} _{-1.217}	7.4229 ^{+2.457} _{-1.393}	8.2437 ^{+0.836} _{-0.736}	8.0143 ^{+1.170} _{-0.594}
1.6–2.0	3.5278 ^{+1.035} _{-0.725}	6.537 ^{+2.749} _{-1.70}	5.6996 ^{+1.316} _{-0.976}	6.036 ^{+2.074} _{-1.159}	6.6937 ^{+0.689} _{-0.681}	6.524 ^{+0.937} _{-0.537}
2.0–2.4	2.7461 ^{+0.817} _{-0.564}	5.1918 ^{+2.213} _{-1.358}	4.2150 ^{+0.963} _{-0.717}	4.5031 ^{+1.592} _{-0.878}	4.9262 ^{+0.453} _{-0.505}	4.8123 ^{+0.677} _{-0.390}

$\overline{\text{NNLL}}$ result decreases the rapidity distribution at NNLO level by 2.99% at the central rapidity region. This hints toward better perturbative convergence and improved reliability of the perturbative series as suggested before by K-factor analysis.

We now compare the seven-point uncertainties of SV + NSV resummed results with the fixed-order results for the rapidity distribution at various orders. From Table IV, we find that the combined uncertainty due to μ_R and μ_F varies between +11.09% and -9.48% at NNLO accuracy, which is a substantial reduction as compared to the uncertainty of (+29.63%, -20.55%) at LO for the central rapidity region, which is as expected. Figure 1 shows that the uncertainty bands for the resummed results are visibly wider in comparison to the corresponding fixed-order predictions up to NLO accuracy. The uncertainty varies between +29.63% and -20.55% for LO, whereas it lies between +41.23% and -25.63% for LO + $\overline{\text{LL}}$ for the central rapidity region. Similarly, the combined scale uncertainty ranges between +32% and -18.48% for NLO + $\overline{\text{NLL}}$, which is higher than (+23.54%, -17.36%) for NLO accuracy around $y = 0$. On the contrary, at NNLO accuracy, we notice that the uncertainty bands become comparable for fixed-order and SV + NSV resummed predictions. For instance, the seven-point scale uncertainty lies in the range (+11.09%, -9.48%) at NNLO accuracy, which is closer to the range (+13.36%, -7.89%) for NNLO + $\overline{\text{NNLL}}$ level at the central rapidity region. This observation, along with earlier noticed improvement in perturbative convergence and reliability by the inclusion of $\overline{\text{NNLL}}$ contribution, makes a strong case for the relevance of SV + NSV resummed predictions. In addition, there is a systematic decrease in the scale uncertainty when we go from LO + $\overline{\text{LL}}$ to NNLO + $\overline{\text{NNLL}}$ accuracy. Also, the higher-order uncertainty bands are completely included within the lower-order uncertainty bands for the resummed predictions. This again indicates that the inclusion of the resummed result makes the perturbative expansion of the rapidity distribution more convergent. Table IV provides the fixed-order as well as SV + NSV resummed results at the central scale $\mu_R = \mu_F = m_H/2$ for different benchmark

rapidity values at various perturbative orders. It also gives the maximum increments and decrements for the corresponding fixed-order and resummed results in the rapidity distribution from the value at the central scale by varying $\{\mu_R, \mu_F\}$ in the range $\{1/4, 1\}m_H$.

The above analysis presents compelling arguments to establish the significance of SV + NSV resummed contributions. Now, in order to understand the behavior of the resummed result with respect to μ_R and μ_F scales in a better way, we study the impact of each scale individually by keeping the other fixed.

2. Uncertainties of the resummed result with respect to μ_R and μ_F

Here, we demonstrate the individual effect of renormalization and factorization scales on the fixed-order and resummed results by keeping one of the scales fixed. We start with Fig. 2 where the fixed-order (left panel) and SV + NSV resummed (right panel) results for the rapidity distribution are plotted as a function of the rapidity y while keeping the factorization scale fixed at $\mu_F = m_H/2$. The bands are obtained by varying the renormalization scale μ_R in the range $\{1/4, 1\}m_H$ around the central scale. We find that, from NLO accuracy onward, the addition of the resummed contribution to the rapidity distribution decreases the μ_R dependency of the result. For instance, the uncertainty due to the μ_R scale lies in the range (+23.54%, -17.36%) for NLO which reduces to (+17.96%, -14.91%) for NLO + $\overline{\text{NLL}}$ accuracy. Likewise, the uncertainty ranges between +7.56% and -7.89% for NNLO + $\overline{\text{NNLL}}$, which is an improvement over (+9.48%, -9.48%) for NNLO order. Additionally, we observe that there is a considerable reduction in the μ_R uncertainty while going from LO + $\overline{\text{LL}}$ to NNLO + $\overline{\text{NNLL}}$ and the higher-order uncertainty bands are included within lower-order uncertainty bands. The above observations are different from what we had seen in Fig. 1 for the seven-point scale variation, where the combined uncertainty bands due to μ_R and μ_F were wider for resummed predictions. This suggests that SV + NSV resummed results have considerable dependence on factorization scale μ_F . To explore these observations in detail,

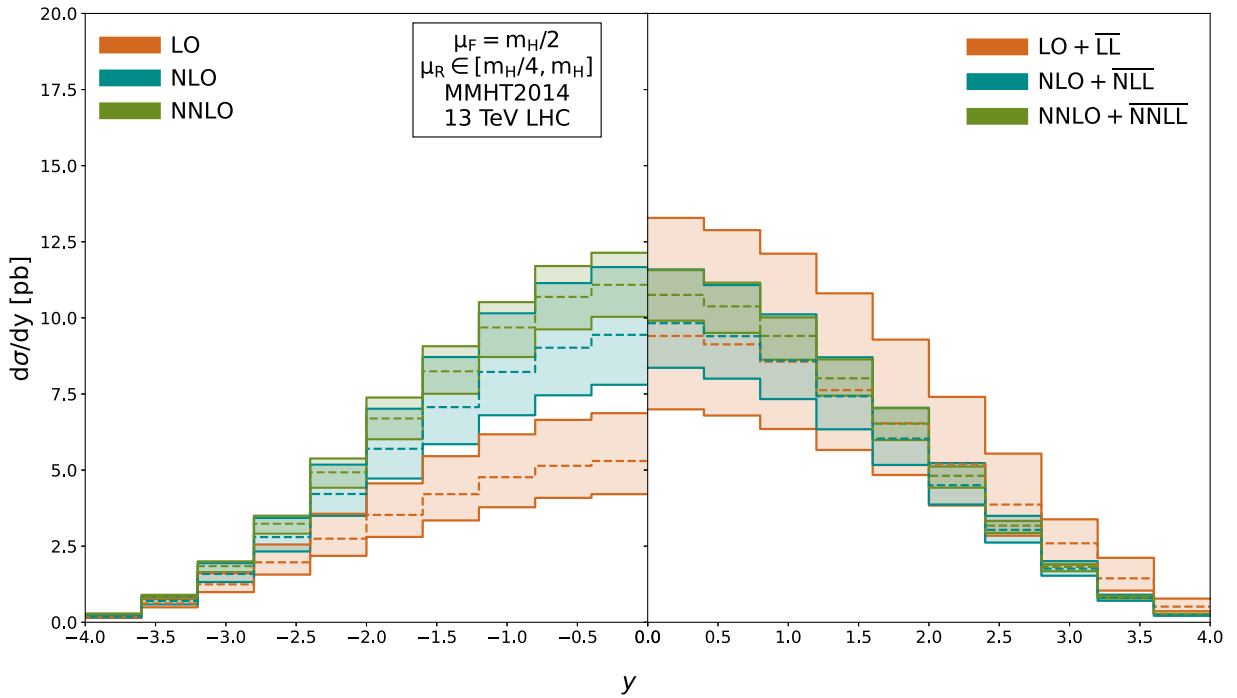


FIG. 2. Comparison of μ_R scale variation between fixed-order and SV + NSV resummed results with the scale $\mu_F = m_H/2$. The dashed lines refer to the corresponding central scale values at each order.

we next study the sensitivity of resummed predictions on factorization scale.

Figure 3 depicts the variation of the fixed-order and SV + NSV resummed predictions with respect to the

factorization (μ_F) scale. The bin-integrated rapidity distribution at various perturbative orders has been plotted against the rapidity y keeping the renormalization scale fixed at $\mu_R = m_H/2$. The uncertainty bands are obtained by

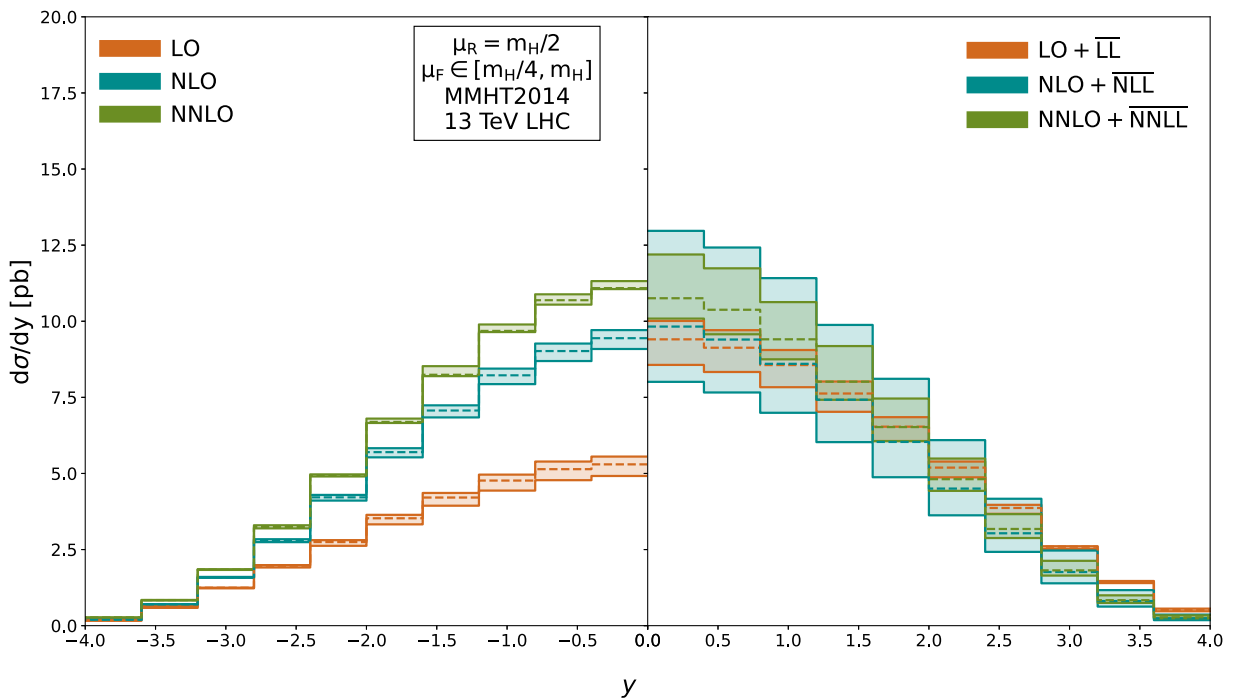


FIG. 3. Comparison of μ_F scale variation between SV and SV + NSV resummed results with the scale $\mu_R = m_H/2$. The dashed lines refer to the corresponding central scale values at each order.

varying μ_F in the range $\{1/4, 1\}m_H$ around the central scale $\mu_R = \mu_F = m_H/2$. We first look at the behavior of fixed-order results (left panel). Interestingly, we see that the uncertainty bands for the fixed-order predictions are very thin, indicating negligible dependence on the factorization scale μ_F . This feature is also evident when we look at the seven-point scale variation (Fig. 1) and μ_R scale variation (Fig. 2) plots of fixed-order results. The similarity between these two plots indicates that the width of the uncertainty band in Fig. 1 is mainly due to the variations in the μ_R scale. On the contrary, the plot for the resummed rapidity distribution (right panel) shows significant dependence on the μ_F scale. The uncertainty due to μ_F variation lies between +6.42% and -8.93% for LO + $\overline{\text{LL}}$ which escalates to (+32%, -18.48%) for NLO + $\overline{\text{NLL}}$ accuracy for the central rapidity region. It comes down to (+13.36%, -6.22%) for NNLO + $\overline{\text{NNLL}}$ level around $y = 0$. If we compare the seven-point variation plot (Fig. 1) and the μ_F variation plot (Fig. 3) for resummed predictions of the rapidity distribution, we find that, from NLO+ $\overline{\text{NLL}}$ level onward, the scale uncertainty is mainly driven by the variation in μ_F .

To summarize, we did a comparative study between fixed-order and SV + NSV resummed predictions for the rapidity distribution. Through the K-factor analysis, we find that the inclusion of resummed results enhances the fixed-order predictions up to NLO accuracy. At NNLO level, the contributions coming from $\overline{\text{NNLL}}$ reduce the fixed-order NNLO prediction, leading to better perturbative convergence and a more reliable result. The study of the behavior of resummed results with respect to the variations in the μ_R scale showed that there is a substantial reduction in the scale dependency as compared to the fixed-order results. However, with respect to the factorization scale, the fixed-order results show negligible dependence, while the addition of resummed contributions increases the sensitivity of the rapidity distribution. The μ_F scale variation is more at NLO + $\overline{\text{NLL}}$ level as compared to NNLO + $\overline{\text{NNLL}}$ accuracy. This behavior of the resummed result with respect to the μ_F variation could be naively attributed to the absence of NSV logarithms coming from the off-diagonal channel. We know that, under the μ_F scale variation, the partonic channels get mixed due to the Dokshitzer-Gribov-Lipatov-Altarelli-Parisi evolution of

the parton distribution functions and compensates among each other to reduce the μ_F dependency. Hence, the lack of off-diagonal resummed NSV logarithms could be the reason for the increased sensitivity of the SV + NSV resummed result. This is not correct because, for Higgs boson production through gluon fusion, the off-diagonal qg channel has a minuscule contribution. To understand the reason behind this, we study the behavior of the SV resummed result in comparison to the SV + NSV resummed result in the next section.

B. SV vs SV + NSV resummed rapidity distribution

In this section, we investigate the impact of inclusion of resummed NSV logarithms by comparing it with the well-established SV resummed results. The analysis in our previous section showed that μ_R scale uncertainty gets improved by adding the SV + NSV resummed contribution to the fixed-order result. Contrary to this, there is a significant increase in the μ_F scale uncertainty by the inclusion of resummed results. Here, we try to understand which part of the SV + NSV resummed result is responsible for the exhibited behavior with respect to the variations in μ_R and μ_F scales.

We first look at the K-factor values given in Table V for SV and SV + NSV resummed results at various perturbative orders for benchmark rapidity values. We find that the inclusion of resummed NSV contributions enhances the rapidity distribution by 7.17% when we go from NLL to $\overline{\text{NLL}}$ accuracy at the central rapidity region. On the other hand, there is a slight reduction of 0.49% in the rapidity distribution when we go from NNLL to $\overline{\text{NNLL}}$ accuracy. We also observe that the K-factor values for NLO + $\overline{\text{NLL}}$ and NNLO + $\overline{\text{NNLL}}$ are closer to each other as compared to the corresponding values at NLO + NLL and NNLO + NNLL. The above observations suggest that the incorporation of resummed NSV contribution to the threshold SV resummed result improves the perturbative convergence of the predictions.

We move on to investigate the uncertainties related to μ_R and μ_F scales arising from the NSV logarithms. We start with the canonical seven-point scale variation plot shown in Fig. 4 for the bin-integrated rapidity distribution of the Higgs boson for SV (left panel) and SV + NSV (right panel) resummed predictions at various perturbative orders.

TABLE V. K-factor values of fixed-order and resummed results at the central scale $\mu_R = \mu_F = m_H/2$.

y	$K_{\text{LO+LL}}$	$K_{\text{LO+LL}}$	$K_{\text{NLO+NLL}}$	$K_{\text{NLO+NLL}}$	$K_{\text{NNLO+NNLL}}$	$K_{\text{NNLO+NNLL}}$
0-0.4	1.453	1.775	1.730	1.854	2.04	2.030
0.4-0.8	1.455	1.776	1.704	1.828	2.028	2.019
0.8-1.2	1.471	1.796	1.679	1.804	1.981	1.973
1.2-1.6	1.484	1.812	1.636	1.763	1.910	1.904
1.6-2.0	1.518	1.853	1.581	1.711	1.851	1.849
2.0-2.4	1.546	1.891	1.508	1.640	1.751	1.752

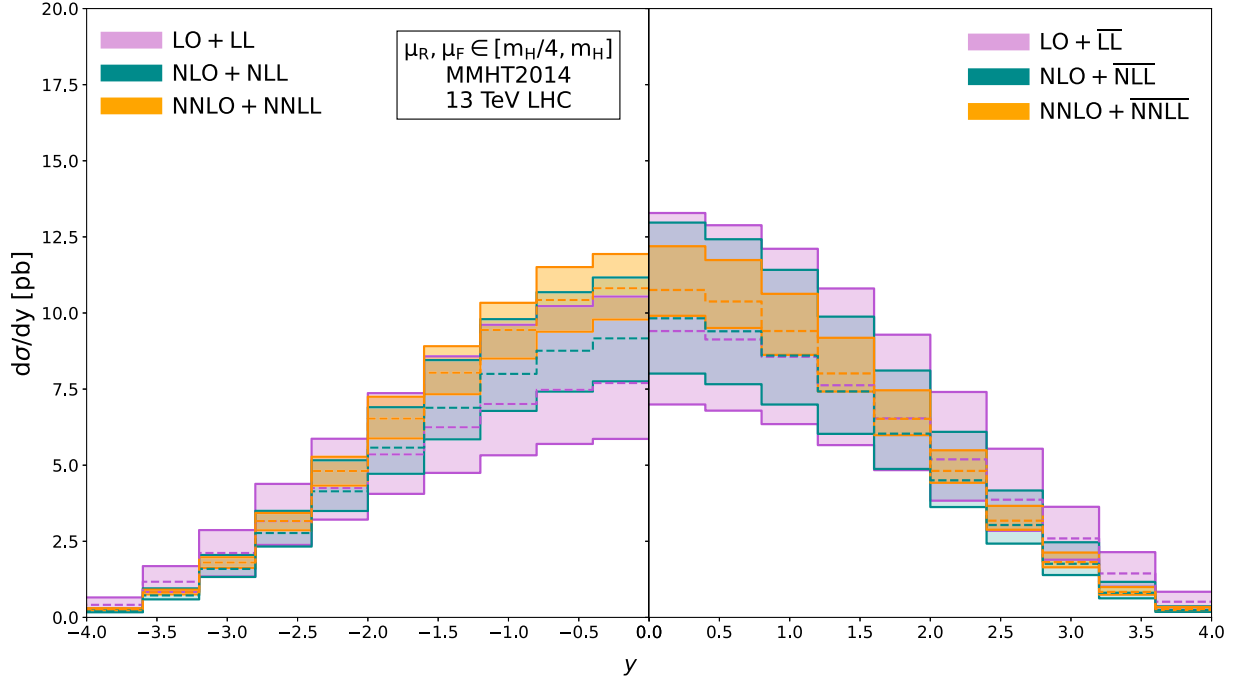


FIG. 4. Comparison of seven-point scale variation between SV and SV + NSV resummed results for 13 TeV LHC. The dashed lines refer to the corresponding central scale values at each order.

The scales $\{\mu_R, \mu_F\}$ are varied in the range $\{m_H/4, m_H\}$, keeping the ratio $\frac{\mu_R}{\mu_F}$ not larger than 2 and smaller than $1/2$ around the central scale value $\mu_R = \mu_F = m_H/2$ for 13 TeV LHC. From Fig. 4, we notice that the addition of resummed NSV contributions to the SV resummed results increases the combined scale uncertainty up to next-to-next-to-leading logarithmic accuracy. However, the difference in the width of uncertainty bands of $\text{NNLO} + \overline{\text{NNLL}}$ and $\text{NNLO} + \text{NNLL}$ is significantly less as compared to that of $\text{NLO} + \overline{\text{NLL}}$ and $\text{NLO} + \text{NLL}$. For instance, the seven-point scale uncertainty at $\text{NLO} + \text{NLL}$ varies between $+21.82\%$ and -15.38% , which is considerably increased to $(+32\%, -18.48\%)$ at $\text{NLO} + \overline{\text{NLL}}$ around the central rapidity region. However, the uncertainty of $(+13.36\%, -7.89\%)$ at $\text{NNLO} + \overline{\text{NNLL}}$ is relatively not too much larger than the uncertainty of $(+10.4\%, -9.48\%)$ at

$\text{NNLO} + \text{NNLL}$ accuracy. We can also see that the uncertainty bands of higher-order SV + NSV resummed results are completely within the lower-order ones over the full rapidity region, which is not the case with SV resummed predictions. This hints toward a more convergent perturbative expansion by the incorporation of resummed NSV logarithms. In Table VI, we have given the rapidity distributions of SV and SV + NSV resummed predictions at central scale $\mu_R = \mu_F = m_H/2$ for benchmark rapidity values, along with the corresponding maximum increments and decrements in the rapidity distribution. The increments and decrements from the central scale values are calculated by varying $\{\mu_R, \mu_F\}$ in the range $\{1/4, 1\}m_H$. The above given percentage uncertainties for various perturbative orders are calculated using values from Table VI.

TABLE VI. Values of resummed rapidity distribution at various orders in comparison to the fixed-order results in picobarn at the central scale $\mu_R = \mu_F = m_H/2$ for 13 TeV LHC.

y	LO + LL	LO + $\overline{\text{LL}}$	NLO + NLL	NLO + $\overline{\text{NLL}}$	NNLO + NNLL	NNLO + $\overline{\text{NNLL}}$
0–0.4	7.6990 ^{+2.840} _{-1.835}	9.406 ^{+3.878} _{-2.411}	9.1660 ^{+2.00} _{-1.410}	9.8252 ^{+3.144} _{-1.816}	10.8117 ^{+1.124} _{-1.025}	10.7559 ^{+1.437} _{-0.849}
0.4–0.8	7.4784 ^{+2.747} _{-1.780}	9.1303 ^{+3.752} _{-2.338}	8.7608 ^{+1.922} _{-1.343}	9.3991 ^{+3.023} _{-1.739}	10.4274 ^{+1.079} _{-1.041}	10.3777 ^{+1.361} _{-0.872}
0.8–1.2	7.0128 ^{+2.599} _{-1.687}	8.561 ^{+3.548} _{-2.211}	8.0011 ^{+1.795} _{-1.217}	8.601 ^{+2.815} _{-1.608}	9.4445 ^{+0.889} _{-0.940}	9.407 ^{+1.222} _{-0.783}
1.2–1.6	6.2455 ^{+2.331} _{-1.499}	7.626 ^{+3.179} _{-1.967}	6.8874 ^{+1.564} _{-1.037}	7.4229 ^{+2.457} _{-1.393}	8.0385 ^{+0.869} _{-0.708}	8.0143 ^{+1.170} _{-0.594}
1.6–2.0	5.3542 ^{+2.012} _{-1.296}	6.537 ^{+2.749} _{-1.70}	5.577 ^{+1.327} _{-0.858}	6.036 ^{+2.074} _{-1.159}	6.5317 ^{+0.716} _{-0.652}	6.524 ^{+0.937} _{-0.537}
2.0–2.4	4.2462 ^{+1.622} _{-1.034}	5.1918 ^{+2.213} _{-1.358}	4.1411 ^{+1.019} _{-0.644}	4.5031 ^{+1.592} _{-0.878}	4.8088 ^{+0.467} _{-0.478}	4.8123 ^{+0.677} _{-0.390}

In the above paragraph, we have compared the SV and SV + NSV resummed results for the seven-point scale variations. We found that the resummed NSV logarithms spoil the combined scale uncertainty, especially at NLO + $\overline{\text{NLL}}$ accuracy. Let us now turn to compare the SV and SV + NSV resummed predictions under the variation of each of these scales individually and try to reason out the behavior exhibited by the resummed NSV logarithms.

We first compare μ_R scale uncertainties of SV and SV + NSV resummed predictions. Figure 5 illustrates the bin-integrated rapidity distributions as a function of y under μ_R scale variation with $\mu_F = m_H/2$ kept fixed for both SV (left panel) and SV + NSV (right panel) resummed results. The bands are obtained by varying $\{\mu_R, \mu_F\}$ in the range $\{1/4, 1\}m_H$ around the central scale $\mu_R = \mu_F = m_H/2$ for 13 TeV LHC. From Fig. 5, we can see that the uncertainty bands for SV + NSV resummed predictions become narrower as compared to the SV resummed result from next-to-leading order onward. Quantitatively, the μ_R scale uncertainty for NLO + $\overline{\text{NLL}}$ varying between +17.96% and -14.91% is less than the corresponding uncertainty of (+19.35%, -15.39%) for NLO + $\overline{\text{NLL}}$ accuracy around $y = 0$. Similarly, the uncertainty of (+7.56%, -7.89%) at NNLO + $\overline{\text{NNLL}}$ due to μ_R scale variation is a considerable reduction from the uncertainty lying between +10.40% and -9.48% at NNLO + $\overline{\text{NNLL}}$ accuracy. As mentioned earlier, the μ_R scale uncertainty for fixed-order results lie in the range (+23.54%, -17.36%) at NLO and for NNLO it varies

between +9.48% and -9.48% around the central rapidity region. These percentages show that, at NLO level, the addition of resummed SV as well as resummed NSV contributions to the fixed-order rapidity distribution improves the renormalization scale uncertainty. This is expected, as the inclusion of higher-order logarithmic corrections within a particular channel leads to a decrease in the sensitivity of the rapidity distribution with respect to the μ_R scale. Nevertheless, the addition of resummed SV contributions to the fixed-order result at NNLO level does not bring any notable change in the μ_R uncertainty. The SV distributions constitute only 15.81% of the Born cross section, whereas NSV logarithms contribute to overall 58.91% of the Born cross section at NNLO for the case of inclusive cross section of Higgs boson production, as shown in Table 2 of Ref. [56]. The same trend is expected to follow for the rapidity distribution of Higgs boson production through gluon fusion as well. Thus, SV contributions being the subdominant contributor is not able to bring any change in the behavior of the fixed-order result in comparison to the μ_R scale variation at NNLO. On the other hand, inclusion of NSV logarithms, which is the dominant contributor at this order, results in significant improvement in the μ_R scale uncertainty of the rapidity distribution. These observations are evident from the percentage uncertainties given above.

Based on the inferences given above, it can be established that the resummed results improve the renormalization scale uncertainty of the rapidity distribution. We would like to mention that the resummed results not only carry the

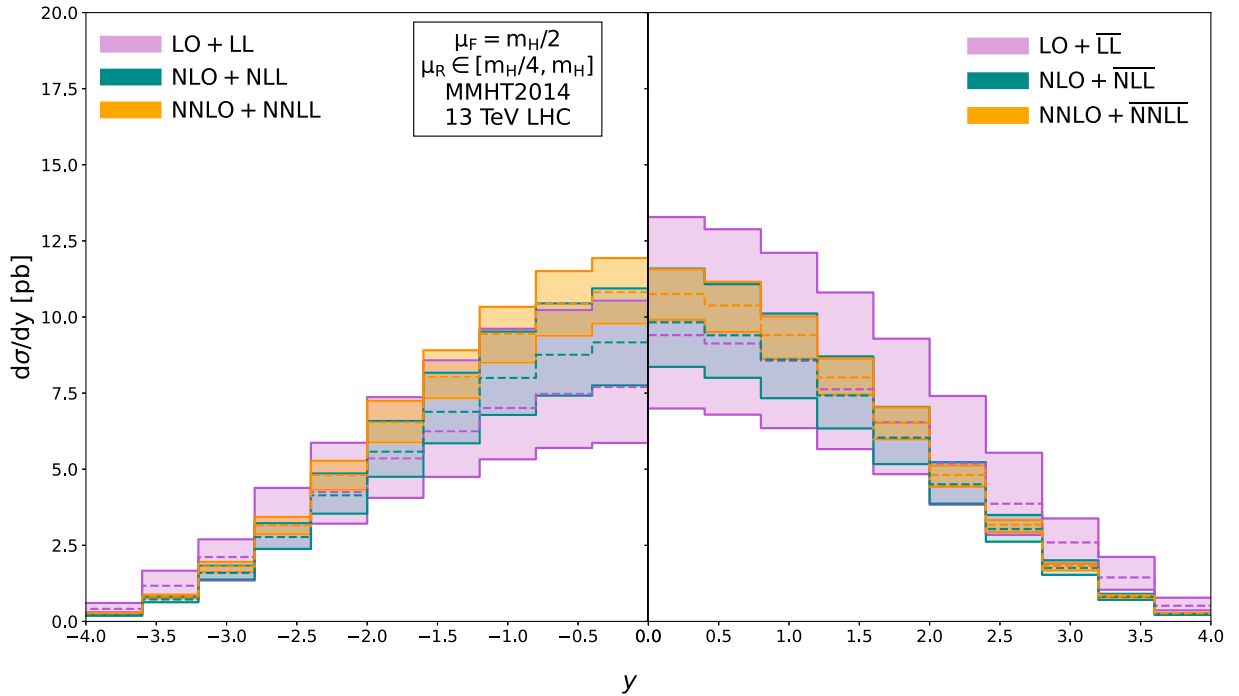


FIG. 5. Comparison of μ_R scale variation between SV and SV + NSV resummed results with the scale $\mu_F = m_H/2$. The dashed lines refer to the corresponding central scale values at each order.

all-order information of the distributions and logarithms that we are resumming, but they also contain certain spurious terms resulting from the “inexact” Mellin inversion of the N space resummed result. These spurious terms are beyond the precision of the resummed quantity. For instance, the resummed SV result at NNLO + NNLL accuracy contains the all-order correction arising from the summation of next-to-next-to-leading towers of SV distributions and, in addition, certain spurious NSV and beyond NSV terms. Similarly, the resummed NSV logarithms at this order contain the all-order correction arising from the summation of next-to-next-to-leading towers of NSV logarithms and certain spurious beyond NSV terms. These spurious terms play an important role in the factorization scale variation of the resummed SV + NSV predictions.

Next, we show the comparison of SV and SV + NSV resummed results for the rapidity distribution under μ_F scale variation. We plot SV (left panel) and SV + NSV (right panel) resummed bin-integrated rapidity distributions as a function of y , keeping the renormalization scale fixed at $\mu_R = m_H/2$ as depicted in Fig. 6. The bands are obtained by varying $\{\mu_R, \mu_F\}$ in the range $\{1/4, 1\}m_H$ around the central scale $\mu_R = \mu_F = m_H/2$ for 13 TeV LHC. We observe that the uncertainty bands of SV + NSV resummed results are wider than the corresponding bands of SV resummed predictions at every order up to NNLO + NNLL. This can be seen quantitatively from the μ_F scale uncertainty of $(+21.82\%, -14.89\%)$ for NLO + NLL which gets escalated to $(+32.0\%, -18.48\%)$ for

NLO + $\overline{\text{NLL}}$ around the central rapidity region. In the same way, the uncertainty lies between $+13.36\%$ and -6.22% for NNLO + $\overline{\text{NNLL}}$, which is a considerable increment over $(+7.63\%, -5.14\%)$ for NNLO + NNLL around $y = 0$.

Let us examine more closely the reason behind the significant dependence of SV as well as SV + NSV resummed results on μ_F scale variation. We consider Fig. 4 given in Ref. [56] for this purpose. We have plotted the fixed-order results truncated to SV + NSV accuracy for the inclusive cross section against μ_F scale variation. We observe that there is a significant dependence of the truncated result on the μ_F scale variation from NLO level onward that escalates at NNLO accuracy. The same behavior is expected to be manifested by the fixed-order results truncated to SV + NSV accuracy for the rapidity distribution as well. Therefore, we compare the behavior of this plot with that of the full fixed-order results under μ_F scale variation, depicted in the left panel of Fig. 3. We find that the μ_F scale dependence of the fixed-order results of the rapidity distribution shown in Fig. 3 is very mild. This indicates that the large μ_F scale variation exhibited by fixed-order results truncated to SV + NSV accuracy is expected to get compensation from beyond NSV terms in the threshold expansion. Figure 4 given in Ref. [56] also suggests that the contributions coming from the beyond NSV terms become more significant with increase in the order of perturbative series. It is because more compensation is required to make the fixed-order predictions almost

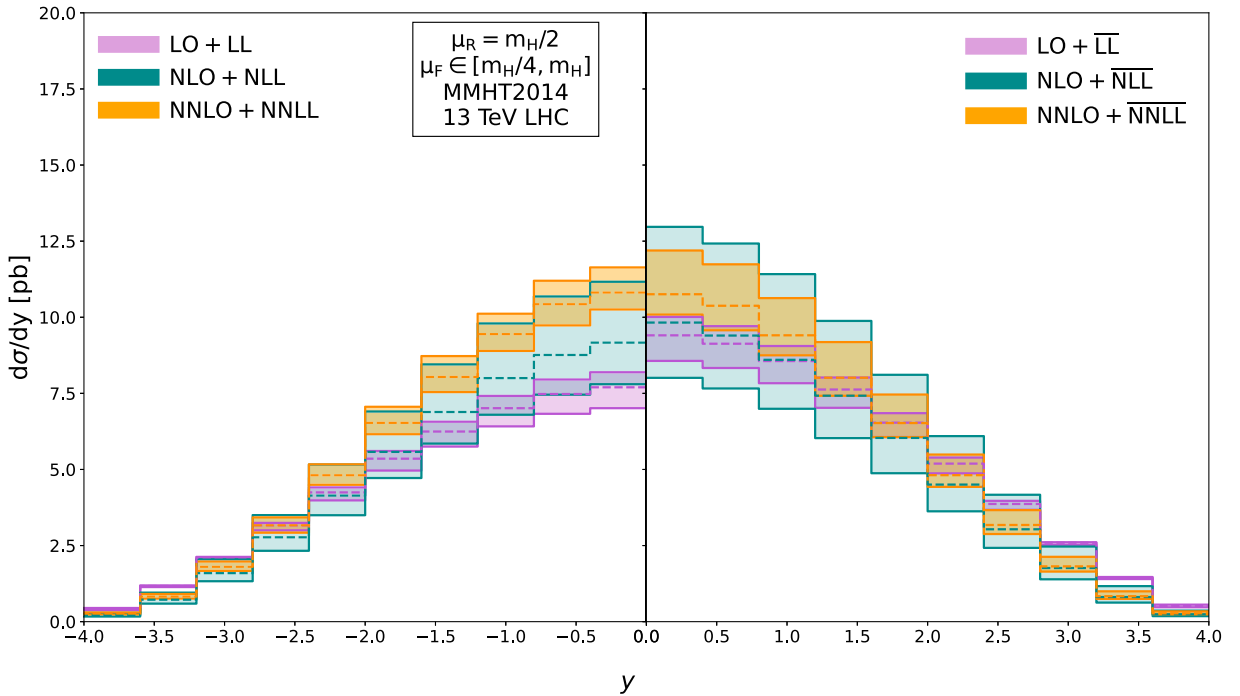


FIG. 6. Comparison of μ_F scale variation between SV and SV + NSV resummed results with the scale $\mu_R = m_H/2$. The dashed lines refer to the corresponding central scale values at each order.

insensitive to the μ_F scale variation as we go to higher orders in the perturbative expansion.

Now, we explore the reason behind the behavior of resummed SV results under μ_F scale variation. The addition of resummed SV contributions to the fixed-order predictions increases the sensitivity of the rapidity distribution with respect to the μ_F scale variation. This can be seen quantitatively from μ_F scale uncertainties varying in the range (+21.82%, -14.89%) and (+7.63%, -5.14%) for NLO + NLL and NNLO + NNLL, respectively, around the central rapidity region. The spurious beyond SV terms resulting from the inexact Mellin inversion of the N space resummed result is mainly responsible for this uncertainty. We also observe that the μ_F scale uncertainty decreases significantly at NNLO + NNLL as compared to NLO + NLL accuracy. This suggests that the resummation of next-to-next-to-leading SV distributions compensates the uncertainty arising from the spurious terms of NLO + NLL with the higher-order logarithmic corrections.

We now proceed to analyze the behavior of NSV logarithms with respect to the μ_F scale variation using the observations made in the above paragraphs for fixed-order and SV resummed results for the rapidity distributions. From Fig. 4 of Ref. [56] and the behavior of fixed-order results under the μ_F variation shown in Fig. 3, we deduced that the μ_F uncertainties due to SV + NSV terms are compensated by uncertainties arising from beyond NSV terms in perturbation theory. We also observed that this compensation increases with the increase in the order of perturbation theory. We know that the SV + NSV resummed predictions contain spurious beyond NSV terms resulting from the resummation of SV as well as NSV parts. The behavior of the resummed SV result showed that the corresponding spurious terms increase the μ_F scale uncertainty of the SV resummed rapidity distribution. Now, with the inclusion of NSV resummed logarithms, there is one additional source to generate spurious beyond NSV terms. Thus, the resummation of NSV logarithms is not supposed to improve the uncertainties arising due to μ_F scale variation of the SV resummed result. This inference is consistent with the plots shown in Fig. 6 where the inclusion of resummed NSV logarithms to the SV resummed result increases the uncertainty due to μ_F scale variation up to NNLO + NNLL accuracy. We also observe that the uncertainty drops down significantly when we go from NLO + NLL to NNLO + NNLL. This suggests that the higher-order logarithmic corrections from the NSV terms improve the μ_F dependency of SV + NSV resummed results. They do so by adding more terms and also by compensating for the spurious NSV terms arising due to SV resummation at lower logarithmic accuracy.

In summary, the renormalization scale dependency of the rapidity distribution decreases by the inclusion of resummed NSV logarithms. This is expected because any change resulting from the μ_R variation gets compensated by the

addition of higher-order terms coming from the resummation of SV and NSV logarithms to all orders. This scenario changes for the case of factorization scale variation. The fixed-order rapidity distribution shows negligible dependence on μ_F scale variation. The addition of SV resummed terms increases the sensitivity of the result with respect to the μ_F scale, which further deteriorates by the inclusion of resummed NSV logarithms. One of the reasons for this behavior is the presence of spurious terms arising due to the inexact Mellin inversion of the N space resummed result. In addition, this significant μ_F dependency of the SV + NSV resummed rapidity distribution is attributed to the lack of beyond NSV terms. This hints toward the importance of beyond NSV terms to get a more accurate and reliable prediction for rapidity distribution. We would also like to mention that we have used the same PDF set for both fixed-order as well as resummed predictions. It is worthwhile to consider resummed PDFs if they are available, especially for studying the variations with respect to μ_F scale.

IV. DISCUSSION AND CONCLUSION

In this article, we provide for the first time the phenomenological predictions for resummed next-to-soft-virtual corrections to the rapidity distribution of Higgs production in gluon fusion up to NNLO + NNLL accuracy. We have used our recent formalism [58] to systematically resum the NSV logarithms arising from the diagonal gluon-gluon (gg) channel to all orders. In our previous work on inclusive Higgs cross section, we have studied the significance of NSV logarithms in the fixed-order predictions [56]. The interesting results and findings of [56] have been an inspiration to study the numerical relevance of these NSV logarithms for the case of rapidity distribution as well.

We have analyzed the numerical effects of SV + NSV higher-order predictions by studying the K-factor values around the central scale $\mu_R = \mu_F = m_H/2$ for benchmark rapidity values. We find that there is an enhancement of 77.5% and 4.04% at LO + LL and NLO + NLL, respectively, by the inclusion of SV + NSV resummed results around the central rapidity region. However, the rapidity distribution at NNLO gets decreased by 2.96% when we include the NNLL resummed corrections at the central rapidity region. This clearly indicates the improvement in the perturbative convergence at NNLO + NNLL accuracy. Furthermore, we notice that the inclusion of higher-order resummed SV + NSV corrections makes the perturbative predictions more reliable due to very small percentage enhancement in the rapidity distribution at NNLO + NNLL in comparison to NLO + NLL for a wide range of rapidity values.

The standard canonical seven-point scale variation approach has been employed to study the dependence of our numerical predictions on renormalization (μ_R) and factorization (μ_F) scales. We have presented the plot of

seven-point scale variation around the central scale $\mu_R = \mu_F = m_H/2$ for 13 TeV LHC. We find that the width of uncertainty bands of resummed predictions is more than that of the corresponding fixed-order results up to NLO. However, for NNLO and NNLO + $\overline{\text{NNLL}}$, the width of the uncertainty bands are comparable. Thus, by performing the seven-point scale variation analysis, we observe that there is a systematic reduction in the uncertainty of the resummed results while going to higher logarithmic accuracy for the central scale $\mu_R = \mu_F = m_H/2$ around the central rapidity region. Moreover, we notice that the uncertainty bands corresponding to higher-order predictions are well contained within that of lower-order ones. This is also an indication of better perturbative convergence attained by the process of resummation.

The detailed analysis of the scale uncertainties unveiled that the seven-point scale uncertainties of SV + NSV resummed predictions are mostly driven by the variations in factorization scale μ_F , especially at NLO + $\overline{\text{NLL}}$. On the other hand, the dependence on the renormalization scale μ_R gets reduced by the inclusion of SV + NSV resummed results leading to more reliable predictions. Furthermore, there is a systematic reduction in the μ_R scale uncertainty while going from LO + $\overline{\text{LL}}$ to NNLO + $\overline{\text{NNLL}}$ due to the addition of higher logarithmic corrections. From the comparison of SV and SV + NSV resummed results, we find that it is the NSV part of the resummation that is

responsible for bringing down the uncertainty due to μ_R scale variation. Thus, the inclusion of more corrections within the same partonic channel improves the μ_R scale uncertainties. This is due to the fact that different channels, being renormalization group invariant, do not mix under μ_R scale variation. However, the uncertainties due to μ_F scale variations get worse by the addition of NSV corrections. From our analysis, we found that the lack of beyond NSV resummed terms is the reason behind the sensitivity of SV + NSV resummed results on μ_F scale variations.

ACKNOWLEDGMENTS

We thank J. Michel and F. Tackmann for third-order results of rapidity for comparison purposes and C. Duhr and B. Mistlberger for providing third-order results for the inclusive reactions. In addition, we would also like to thank the members of the computer administrative unit of IMSC for their help and support.

APPENDIX A: NSV RESUMMATION

EXPONENTS $\bar{g}_{d,i}^g(\omega)$

The NSV resummation exponents $\bar{g}_{d,i}^g(\omega)$ given in (21) are provided as follows:

$$\bar{g}_{d,1}^g(\omega) = \frac{1}{\beta_0} C_A \{2L_\omega\}, \quad (\text{A1})$$

$$\bar{g}_{d,2}^g(\omega) = \frac{\beta_1}{\beta_0^2} C_A \{2\omega + 2L_\omega\} + \frac{1}{\beta_0} C_A n_f \left\{ \frac{20}{9} \omega \right\} + \frac{1}{\beta_0} C_A^2 \left\{ -\frac{134}{9} \omega + 4\omega\zeta_2 \right\} + C_A \{-2 + 2L_{qr} - 2L_{fr} + 2L_{fr}\omega - 4\gamma_E\}, \quad (\text{A2})$$

$$\begin{aligned} \bar{g}_{d,3}^g(\omega) = & \frac{\beta_1^2}{\beta_0^3} C_A \{\omega^2 - L_\omega^2\} + \frac{\beta_2}{\beta_0^2} C_A \{-\omega^2\} + \frac{\beta_1}{\beta_0^2} C_A n_f \left\{ -\frac{20}{9} \omega + \frac{10}{9} \omega^2 - \frac{20}{9} L_\omega \right\} + \frac{\beta_1}{\beta_0^2} C_A^2 \left\{ \frac{134}{9} \omega - 4\omega\zeta_2 - \frac{67}{9} \omega^2 \right. \\ & + 2\omega^2\zeta_2 + \frac{134}{9} L_\omega - 4L_\omega\zeta_2 \left. \right\} + \frac{1}{\beta_0} C_A n_f^2 \left\{ \frac{8}{27} \omega - \frac{4}{27} \omega^2 \right\} + \frac{1}{\beta_0} C_A C_F n_f \left\{ \frac{55}{3} \omega - 16\omega\zeta_3 - \frac{55}{6} \omega^2 + 8\omega^2\zeta_3 \right\} \\ & + \frac{1}{\beta_0} C_A^2 n_f \left\{ \frac{418}{27} \omega + \frac{56}{3} \omega\zeta_3 - \frac{80}{9} \omega\zeta_2 - \frac{209}{27} \omega^2 - \frac{28}{3} \omega^2\zeta_3 + \frac{40}{9} \omega^2\zeta_2 \right\} \\ & + \frac{1}{\beta_0} C_A^3 \left\{ -\frac{245}{3} \omega - \frac{44}{3} \omega\zeta_3 + \frac{536}{9} \omega\zeta_2 - \frac{88}{5} \omega\zeta_2^2 + \frac{245}{6} \omega^2 + \frac{22}{3} \omega^2\zeta_3 - \frac{268}{9} \omega^2\zeta_2 + \frac{44}{5} \omega^2\zeta_2^2 \right\} \\ & + \frac{\beta_1}{\beta_0} C_A \{2L_\omega - 2L_\omega L_{qr} + 4L_\omega\gamma_E\} + C_A n_f \left\{ \frac{116}{27} - \frac{2}{3} \zeta_2 - \frac{20}{9} L_{qr} + \frac{20}{9} L_{fr} - \frac{40}{9} L_{fr}\omega + \frac{20}{9} L_{fr}\omega^2 + \frac{40}{9} \gamma_E \right\} \\ & + C_A^2 \left\{ -\frac{806}{27} + 14\zeta_3 + \frac{23}{3} \zeta_2 + \frac{134}{9} L_{qr} - 4L_{qr}\zeta_2 - \frac{134}{9} L_{fr} + 4L_{fr}\zeta_2 + \frac{268}{9} L_{fr}\omega - 8L_{fr}\omega\zeta_2 \right. \\ & \left. - \frac{134}{9} L_{fr}\omega^2 + 4L_{fr}\omega^2\zeta_2 - \frac{268}{9} \gamma_E + 8\gamma_E\zeta_2 \right\} \\ & + \beta_0 C_A \{-\zeta_2 + 2L_{qr} - L_{qr}^2 + L_{fr}^2 - 2L_{fr}^2\omega + L_{fr}^2\omega^2 - 4\gamma_E + 4\gamma_E L_{qr} - 4\gamma_E^2\}. \end{aligned} \quad (\text{A3})$$

APPENDIX B: NSV RESUMMATION EXPONENTS $h_{d,ij}^g(\omega)$ AND $\tilde{h}_{d,ii}^g(\omega, \omega_l)$

The NSV resummation exponents $h_{d,ij}^g(\omega)$ and $\tilde{h}_{d,ii}^g(\omega, \omega_l)$ given in (22) are provided as follows:

$$h_{d,00}^g(\omega) = \frac{1}{\beta_0} C_A \{-4L_\omega\} h_{d,01}^g(\omega) = 0, \quad (\text{B1})$$

$$h_{d,10}^g(\omega) = \frac{1}{2\beta_0^2(\omega-1)} \left[\beta_1 C_A \{8\omega + 8L_\omega\} + \beta_0 C_A n_f \left\{ \frac{80}{9} \omega \right\} + \beta_0 C_A^2 \left\{ -\frac{536}{9} \omega + 16\omega\zeta_2 - 32\gamma_E \omega \right\} \right. \\ \left. + \beta_0^2 C_A \{-4 - 8L_{fr} + 8L_{fr}\omega + 8L_{qr} - 16\gamma_E\} \right], \quad (\text{B2})$$

$$\tilde{h}_{d,11}^g(\omega, \omega_l) = \frac{C_A^2}{\beta_0} \left\{ -\frac{4\omega_l}{(\omega-1)^2} - \frac{16\omega}{(\omega-1)} \right\}, \quad (\text{B3})$$

$$h_{d,20}^g(\omega) = \frac{1}{2\beta_0^3(\omega-1)^2} \left[\beta_1^2 C_A \{-4\omega^2 + 4L_\omega^2\} + \beta_0 \beta_2 C_A \{4\omega^2\} + \beta_0 \beta_1 C_A n_f \left\{ \frac{80}{9} \omega - \frac{40}{9} \omega^2 + \frac{80}{9} L_\omega \right\} \right. \\ \left. + \beta_0 \beta_1 C_A^2 \left\{ -\frac{536}{9} \omega + 16\omega\zeta_2 + \frac{268}{9} \omega^2 - 8\omega^2\zeta_2 - 32\gamma_E \omega + 16\gamma_E \omega^2 - \frac{536}{9} L_\omega + 16L_\omega\zeta_2 - 32L_\omega\gamma_E \right\} \right. \\ \left. + \beta_0^2 C_A n_f^2 \left\{ -\frac{32}{27} \omega + \frac{16}{27} \omega^2 \right\} + \beta_0^2 C_A C_{Fnf} \left\{ -\frac{172}{3} \omega + 64\omega\zeta_3 + \frac{86}{3} \omega^2 - 32\omega^2\zeta_3 \right\} \right. \\ \left. + \beta_0^2 C_A^2 n_f \left\{ -\frac{1096}{27} \omega - \frac{224}{3} \omega\zeta_3 + \frac{320}{9} \omega\zeta_2 + \frac{548}{27} \omega^2 + \frac{112}{3} \omega^2\zeta_3 - \frac{160}{9} \omega^2\zeta_2 - \frac{640}{9} \gamma_E \omega + \frac{320}{9} \gamma_E \omega^2 \right\} \right. \\ \left. + \beta_0^2 C_A^3 \left\{ \frac{724}{3} \omega - \frac{112}{3} \omega\zeta_3 - \frac{2144}{9} \omega\zeta_2 + \frac{352}{5} \omega\zeta_2^2 - \frac{362}{3} \omega^2 + \frac{56}{3} \omega^2\zeta_3 + \frac{1072}{9} \omega^2\zeta_2 - \frac{176}{5} \omega^2\zeta_2^2 + \frac{4288}{9} \gamma_E \omega \right. \right. \\ \left. \left. - 128\gamma_E \omega\zeta_2 - \frac{2144}{9} \gamma_E \omega^2 + 64\gamma_E \omega^2\zeta_2 \right\} + \beta_0^2 \beta_1 C_A \{8\omega - 4\omega^2 - 4L_\omega + 8L_\omega L_{qr} - 16L_\omega \gamma_E\} \right. \\ \left. + \beta_0^3 C_A n_f \left\{ -\frac{272}{27} + \frac{32}{3} \zeta_2 - \frac{80}{9} L_{fr} + \frac{160}{9} L_{fr}\omega - \frac{80}{9} L_{fr}\omega^2 + \frac{80}{9} L_{qr} - \frac{148}{9} \gamma_E \right\} \right. \\ \left. + \beta_0^3 C_A^2 \left\{ \frac{1808}{27} - 56\zeta_3 - \frac{224}{3} \zeta_2 + \frac{536}{9} L_{fr} - 16L_{fr}\zeta_2 - \frac{1072}{9} L_{fr}\omega + 32L_{fr}\omega\zeta_2 + \frac{536}{9} L_{fr}\omega^2 - 16L_{fr}\omega^2\zeta_2 \right. \right. \\ \left. \left. - \frac{536}{9} L_{qr} + 16L_{qr}\zeta_2 + \frac{1060}{9} \gamma_E - 32\gamma_E\zeta_2 + 32\gamma_E L_{fr} - 64\gamma_E L_{fr}\omega + 32\gamma_E L_{fr}\omega^2 - 32\gamma_E L_{qr} + 56\gamma_E^2 \right\} \right. \\ \left. + \beta_0^4 C_A \{16\zeta_2 - 4L_{fr}^2 + 8L_{fr}^2\omega - 4L_{fr}^2\omega^2 - 4L_{qr} + 4L_{qr}^2 + 8\gamma_E - 16\gamma_E L_{qr} + 16\gamma_E^2\} \right], \quad (\text{B4})$$

$$h_{d,21}^g(\omega) = \frac{1}{2\beta_0^2(\omega-1)^2} \left[\beta_1 C_A^2 \{-32\omega + 16\omega^2 - 32L_\omega\} + \beta_0 C_A^2 n_f \left\{ -\frac{640}{9} \omega + \frac{320}{9} \omega^2 \right\} \right. \\ \left. + \beta_0 C_A^3 \left\{ \frac{4288}{9} \omega - 128\omega\zeta_2 - \frac{2144}{9} \omega^2 + 64\omega^2\zeta_2 \right\} + \beta_0^2 C_A n_f \left\{ \frac{4}{3} \right\} \right. \\ \left. + \beta_0^2 C_A^2 \left\{ -\frac{4}{3} + 32L_{fr} - 64L_{fr}\omega + 32L_{fr}\omega^2 - 32L_{qr} + 48\gamma_E \right\} \right], \quad (\text{B5})$$

$$\tilde{h}_{d,22}^g(\omega, \omega_l) = \frac{\omega_l}{\beta_0(\omega-1)^3} \left[C_A^2 n_f \left\{ \frac{32}{27} \right\} + C_A^3 \left\{ -\frac{176}{27} \right\} \right], \quad (\text{B6})$$

where γ_E is the Euler-Mascheroni constant. Here, $L_\omega = \ln(1-\omega)$ with $\omega = \beta_0 a_s(\mu_R^2) \ln N_1 N_2$, $\omega_l = \beta_0 a_s(\mu_R^2) \ln N_l$ with $l = 1, 2$, $L_{qr} = \ln\left(\frac{q^2}{\mu_R^2}\right)$, and $L_{fr} = \ln\left(\frac{f^2}{\mu_R^2}\right)$.

- [1] G. Aad *et al.* (ATLAS Collaboration), *Phys. Lett. B* **716**, 1 (2012).
- [2] S. Chatrchyan *et al.* (CMS Collaboration), *Phys. Lett. B* **716**, 30 (2012).
- [3] T. Affolder *et al.* (CDF Collaboration), *Phys. Rev. D* **63**, 011101 (2001).
- [4] F. Abe *et al.* (CDF Collaboration), *Phys. Rev. Lett.* **81**, 5754 (1998).
- [5] V. Khachatryan *et al.* (CMS Collaboration), *Eur. Phys. J. C* **75**, 147 (2015).
- [6] T. Affolder *et al.* (CDF Collaboration), *Phys. Rev. Lett.* **87**, 131802 (2001).
- [7] N. Arkani-Hamed, S. Dimopoulos, and G. R. Dvali, *Phys. Lett. B* **429**, 263 (1998).
- [8] L. Randall and R. Sundrum, *Phys. Rev. Lett.* **83**, 3370 (1999).
- [9] J. Gao, M. Guzzi, J. Huston, H.-L. Lai, Z. Li, P. Nadolsky, J. Pumplin, D. Stump, and C.-P. Yuan, *Phys. Rev. D* **89**, 033009 (2014).
- [10] L. A. Harland-Lang, A. D. Martin, P. Motylinski, and R. S. Thorne, *Eur. Phys. J. C* **75**, 204 (2015).
- [11] R. D. Ball *et al.* (NNPDF Collaboration), *J. High Energy Phys.* **04** (2015) 040.
- [12] J. Butterworth *et al.*, *J. Phys. G* **43**, 023001 (2016).
- [13] S. Alekhin, J. Blumlein, S. Moch, and R. Placakyte, *Phys. Rev. D* **96**, 014011 (2017).
- [14] C. Duhr, F. Dulat, and B. Mistlberger, *Phys. Rev. Lett.* **125**, 172001 (2020).
- [15] T. Ahmed, M. Mahakhud, N. Rana, and V. Ravindran, *Phys. Rev. Lett.* **113**, 112002 (2014).
- [16] C. Anastasiou, C. Duhr, F. Dulat, F. Herzog, and B. Mistlberger, *Phys. Rev. Lett.* **114**, 212001 (2015).
- [17] Y. Li, A. von Manteuffel, R. M. Schabinger, and H. X. Zhu, *Phys. Rev. D* **90**, 053006 (2014).
- [18] S. Catani, L. Cieri, D. de Florian, G. Ferrera, and M. Grazzini, *Nucl. Phys.* **B888**, 75 (2014).
- [19] C. Duhr, F. Dulat, and B. Mistlberger, *Phys. Rev. Lett.* **125**, 051804 (2020).
- [20] T. Ahmed, M. K. Mandal, N. Rana, and V. Ravindran, *J. High Energy Phys.* **02** (2015) 131.
- [21] G. F. Sterman, *Nucl. Phys.* **B281**, 310 (1987).
- [22] S. Catani and L. Trentadue, *Nucl. Phys.* **B327**, 323 (1989).
- [23] S. Catani and L. Trentadue, *Nucl. Phys.* **B353**, 183 (1991).
- [24] S. Moch and A. Vogt, *Phys. Lett. B* **631**, 48 (2005).
- [25] E. Laenen and L. Magnea, *Phys. Lett. B* **632**, 270 (2006).
- [26] A. Idilbi, X.-d. Ji, J.-P. Ma, and F. Yuan, *Phys. Rev. D* **73**, 077501 (2006).
- [27] V. Ravindran, *Nucl. Phys.* **B746**, 58 (2006).
- [28] V. Ravindran, *Nucl. Phys.* **B752**, 173 (2006).
- [29] V. Ravindran, J. Smith, and W. L. van Neerven, *Nucl. Phys.* **B767**, 100 (2007).
- [30] V. Ravindran and J. Smith, *Phys. Rev. D* **76**, 114004 (2007).
- [31] T. Ahmed, M. K. Mandal, N. Rana, and V. Ravindran, *Phys. Rev. Lett.* **113**, 212003 (2014).
- [32] P. Banerjee, G. Das, P. K. Dhani, and V. Ravindran, *Phys. Rev. D* **97**, 054024 (2018).
- [33] P. Banerjee, G. Das, P. K. Dhani, and V. Ravindran, *Phys. Rev. D* **98**, 054018 (2018).
- [34] A. Idilbi and X.-d. Ji, *Phys. Rev. D* **72**, 054016 (2005).
- [35] T. Becher and M. Neubert, *Eur. Phys. J. C* **71**, 1665 (2011).
- [36] T. Becher and M. Neubert, *Phys. Rev. Lett.* **97**, 082001 (2006).
- [37] T. Becher, M. Neubert, and G. Xu, *J. High Energy Phys.* **07** (2008) 030.
- [38] M. Bonvini, S. Forte, G. Ridolfi, and L. Rottoli, *J. High Energy Phys.* **01** (2015) 046.
- [39] C. Anastasiou, C. Duhr, F. Dulat, F. Herzog, and B. Mistlberger, *Phys. Rev. Lett.* **114**, 212001 (2015).
- [40] F. Dulat, B. Mistlberger, and A. Pelloni, *Phys. Rev. D* **99**, 034004 (2019).
- [41] E. Laenen, L. Magnea, and G. Stavenga, *Phys. Lett. B* **669**, 173 (2008).
- [42] E. Laenen, L. Magnea, G. Stavenga, and C. D. White, *J. High Energy Phys.* **01** (2011) 141.
- [43] D. Bonocore, E. Laenen, L. Magnea, L. Vernazza, and C. D. White, *Phys. Lett. B* **742**, 375 (2015).
- [44] D. Bonocore, E. Laenen, L. Magnea, S. Melville, L. Vernazza, and C. White, *J. High Energy Phys.* **06** (2015) 008.
- [45] D. Bonocore, E. Laenen, L. Magnea, L. Vernazza, and C. White, *J. High Energy Phys.* **12** (2016) 121.
- [46] V. Del Duca, E. Laenen, L. Magnea, L. Vernazza, and C. White, *J. High Energy Phys.* **11** (2017) 057.
- [47] N. Bahjat-Abbas, D. Bonocore, J. Sinninghe Damsté, E. Laenen, L. Magnea, L. Vernazza, and C. White, *J. High Energy Phys.* **11** (2019) 002.
- [48] G. Soar, S. Moch, J. Vermaseren, and A. Vogt, *Nucl. Phys.* **B832**, 152 (2010).
- [49] S. Moch and A. Vogt, *J. High Energy Phys.* **11** (2009) 099.
- [50] D. de Florian, J. Mazzitelli, S. Moch, and A. Vogt, *J. High Energy Phys.* **10** (2014) 176.
- [51] M. Beneke, A. Broggio, M. Garny, S. Jaskiewicz, R. Szafron, L. Vernazza, and J. Wang, *J. High Energy Phys.* **03** (2019) 043.
- [52] M. Beneke, M. Garny, S. Jaskiewicz, R. Szafron, L. Vernazza, and J. Wang, *J. High Energy Phys.* **01** (2020) 094.
- [53] M. Beneke, A. Broggio, S. Jaskiewicz, and L. Vernazza, *J. High Energy Phys.* **07** (2020) 078.
- [54] A. Ajjath, P. Mukherjee, and V. Ravindran, *Phys. Rev. D* **105**, 094035 (2022).
- [55] A. Ajjath, P. Mukherjee, V. Ravindran, A. Sankar, and S. Tiwari, *J. High Energy Phys.* **04** (2021) 131.
- [56] A. H. Ajjath, P. Mukherjee, V. Ravindran, A. Sankar, and S. Tiwari, *Eur. Phys. J. C* **82**, 774 (2022).
- [57] A. H. Ajjath, P. Mukherjee, V. Ravindran, A. Sankar, and S. Tiwari, *Eur. Phys. J. C* **82**, 234 (2022).
- [58] A. H. Ajjath, P. Mukherjee, V. Ravindran, A. Sankar, and S. Tiwari, *Phys. Rev. D* **103**, L111502 (2021).
- [59] M. Gerlach, F. Herren, and M. Steinhauser, *J. High Energy Phys.* **11** (2018) 141.
- [60] K. G. Chetyrkin, B. A. Kniehl, M. Steinhauser, and W. A. Bardeen, *Nucl. Phys.* **B535**, 3 (1998).
- [61] G. Altarelli and G. Parisi, *Nucl. Phys.* **B126**, 298 (1977).
- [62] S. Moch, J. A. M. Vermaseren, and A. Vogt, *Nucl. Phys.* **B688**, 101 (2004).
- [63] A. Vogt, S. Moch, and J. A. M. Vermaseren, *Nucl. Phys.* **B691**, 129 (2004).
- [64] J. Blümlein, P. Marquard, C. Schneider, and K. Schönwald, *Nucl. Phys.* **B971**, 115542 (2021).

- [65] P. Banerjee, P. K. Dhani, M. C. Kumar, P. Mathews, and V. Ravindran, *Phys. Rev. D* **97**, 094028 (2018).
- [66] T. Ahmed, A. A. H., P. Mukherjee, V. Ravindran, and A. Sankar, *Eur. Phys. J. C* **81**, 943 (2021).
- [67] V. Ravindran, J. Smith, and W. L. van Neerven, *Nucl. Phys.* **B665**, 325 (2003).
- [68] B. Mistlberger, *J. High Energy Phys.* 05 (2018) 028.
- [69] P. A. Zyla *et al.* (Particle Data Group), *Prog. Theor. Exp. Phys.* **2020**, 083C01 (2020).
- [70] C. Anastasiou, K. Melnikov, and F. Petriello, *Nucl. Phys.* **B724**, 197 (2005).
- [71] S. Catani, M. L. Mangano, P. Nason, and L. Trentadue, *Nucl. Phys.* **B478**, 273 (1996).
- [72] A. Buckley, J. Ferrando, S. Lloyd, K. Nordström, B. Page, M. Rüfenacht, M. Schönherr, and G. Watt, *Eur. Phys. J. C* **75**, 132 (2015).
- [73] A. Vogt, *Comput. Phys. Commun.* **170**, 65 (2005).
- [74] S. Catani, D. de Florian, M. Grazzini, and P. Nason, *J. High Energy Phys.* 07 (2003) 028.
- [75] A. H. Ajjath, P. Mukherjee, V. Ravindran, A. Sankar, and S. Tiwari, *Phys. Rev. D* **106**, 034005 (2022).